COP AND CAPACITY IMPROVEMENT THROUGH WORK AND HEAT RECOVERY BY USING VORTEX TUBE

BY

MUHAMMAD REAZ MOHIUDDIN

THESIS

Submitted in partial fulfillment of the requirements
for the degree of Master of Science in Mechanical Engineering
in the Graduate College of the
University of Illinois at Urbana-Champaign, 2014

Urbana, Illinois

Advisers:

Professor Predrag Stojan Hrnjak
Professor Stefan Elbel

ABSTRACT

The vortex tube is an intriguing device that separates an incoming high-pressure fluid stream into two low-pressure streams. Work interaction during the expansion process causes a temperature decrease in one of the two exit streams, while the other one experiences a temperature increase. The expansion process in a vortex tube therefore approaches isentropic rather than isenthalpic expansion, and the internal flow separation is achieved without any moving parts, resulting in robust and inexpensive designs. Commercially available vortex tubes are almost exclusively used for spot cooling in industrial applications and use compressed air as the working fluid. In addition, vortex tubes have been gaining lots of attention in air-conditioning and refrigeration research, because of the possibility to replace the expansion valve of vapor compression systems with this low-cost device that can recover expansion work that would otherwise be lost in the isenthalpic throttling process.

Most of the work on vortex tubes used for refrigeration have been numerical studies, and many of them predict very optimistic energy efficiency improvements. However, the few papers available that describe experimental validation of vortex tubes in HVAC&R systems are far less optimistic, which is often caused by the selection of cycle architectures that seem inappropriate for vortex tubes. This thesis takes a fresh look at performance of commercially available vortex tubes with refrigerant and its possible application in refrigeration. A new experimental facility is developed to assess vortex tube performance on a fundamental level for different working fluids, including air and R134a. Suitable vortex tube operating conditions have been identified and efficiencies have been calculated from experimental results for both air and R134a. Experimental investigations show that the vortex tube using high pressure saturated R134a vapor at inlet can achieve up to 35% isentropic efficiency while creating a temperature difference of 18°C between the two low-pressure outlet streams. Based on these new find-

ings, numerical simulation is carried out to investigate the performance of a novel vortex tube cycle that is able to utilize the demonstrated improvement potentials when applied to vapor compression systems. The cycle utilizes temperature separation capability of vortex tube to achieve higher subcooling at evaporator inlet to increase system COP and reduce refrigerant mass flow rate through the system.

To my parents, for their sacrifice in letting me leave them in their old age for my higher studies. To my wife, for her relentless support in the face of perilous hardships

ACKNOWLEDGMENTS

I would like to express my deepest gratitude to my advisors Professor Predrag S. Hrnjak and Professor Stefan Elbel. It is their excellent guidance, endless encouragement and untiring patience throughout my entire time as a graduate student made this project a reality. I am thankful to them for training me to learn how to conduct research with proper planning, resource management and present the results in useful way.

I would also like to thank the members of research group Mr. Neal D. Lawrence and Mr. Augusto J. P. Zimmermann for their insightful comments, suggestions and hands on training that helped improving my work considerably.

This study would not have been possible without the support of the Air Conditioning and Refrigeration Center (ACRC) at the University of Illinois at Urbana-Champaign. Special thanks to all the industrial partners who provided support, encouragement and showed great interest in the project.

In the end, I would like to thank my family, friends and colleagues for their continuous encouragement, constructive criticism and wisdom.

TABLE OF CONTENTS

LIST OF TABLES

LIST OF FIGURES

NOMENCLATURE

Symbols

k	ratio of constant pressure and constant volume specific heat	[-]
c_p	specific heat	[Jkg^{-1}K^{-1}]
$\dot{m}$	mass flow rate of fluid stream	[kg s^{-1}]
N_{rp}	refrigerant pump speed	[Hz]
P	pressure	[kPa]
$\dot{Q}$	thermal capacity	[W]
s	specific entropy	[J kg^{-1} K^{-1}]
T	temperature	[$^{\circ}$C]
W	work done on the system or extracted from system	[W]
y	mass fraction	[-]

Abbreviations

COP	coefficient of performance

Greek symbols

η	efficiency

Subscripts

act	referring to actual condition of the system
avg	referring to averaged value
baseline	referring to vapor compression refrigeration cycle
c	referring to cold fluid stream outlet of vortex tube
cp	referring to compressor
cr	referring to condenser
car	referring to Carnot cycle
cro	referring to condenser outlet
er	referring to evaporator
exp	referring to the expansion process
h	referring to hot fluid stream outlet of vortex tube
is	referring to an isentropic process of ideal gas
isen	referring to an isentropic process of non-ideal gas
o	referring to inlet fluid stream to vortex tube
rp	referring to refrigerant pump
rpi	referring to refrigerant pump inlet
sat	referring to saturated condition
sup	referring to superheated condition
VTsubcool	referring to novel vortex tube cycle with subcooling

CHAPTER 1

INTRODUCTION

1.1 Background

In vapor compression refrigeration cycle, throttling devices such as capillary tubes, short tube orifices and expansion valves are used as robust and cost-effective solution for expanding the refrigerant from higher condenser pressure to lower evaporator pressure. However, the physical process during throttling is irreversible, isenthalpic which inflicts a dual penalty on the system in the form of reduction in cooling capacity as well as increase in required compression work. This results in a decrease in COP of the actual vapor compression refrigeration cycle compared to an ideal Carnot refrigeration cycle. This can be understood by comparing the $T-s$ diagrams for the ideal Carnot refrigeration cycle in Figure 1.1 and its modified versions shown in Figures 1.2 and 1.3 for actual use.

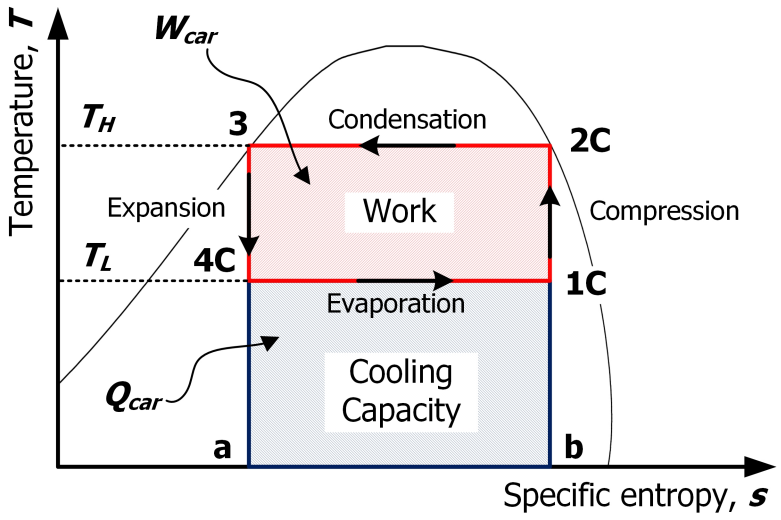

Figure 1.1: Carnot refrigeration cycle $T-s$ diagram

In the ideal Carnot refrigeration cycle $T-s$ diagram shown in Figure 1.1, area 1C-4C-a-b represents the amount of heat removed for the object or space to be cooled and area 1C-2C-3-4C is the work required to drive the cycle. The ratio of the two areas is the COP of the Carnot refrigeration cycle which can be expressed as Equation 1.1.

$$COP_{car} = \frac{Q_{car}}{W_{car}} \tag{1.1}$$

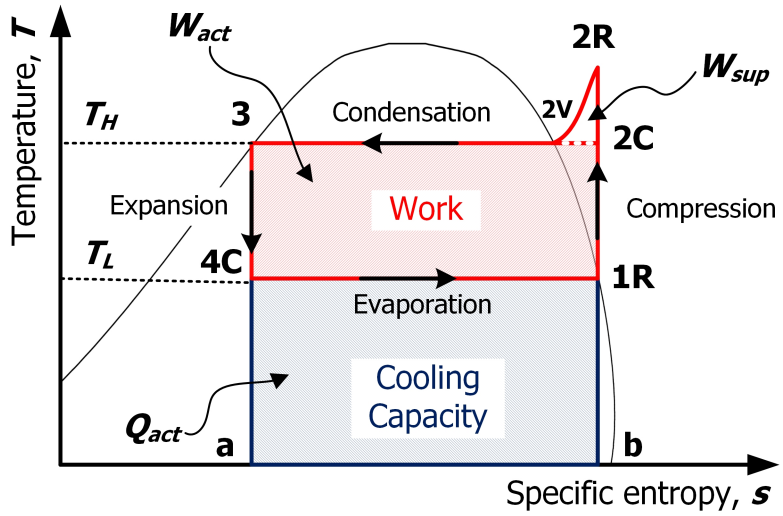

Figure 1.2: Modified Carnot cycle $T-s$ diagram with saturated evaporator outlet

Figure 1.2 shows a modified Carnot cycle with saturated evaporator outlet. The problem of 'wet compression' process 1C-2C of Carnot refrigeration cycle as shown in Figure 1.1 is avoided by saturating the evaporator outlet from point 1C in Figure 1.1 to point 1R in Figure 1.2, as the compressor can only compress vapor in actual systems. Therefore, in actual systems, the compression process carries along 1R-2R as shown in Figure 1.2. This deviation incorporates additional work requirement of W_{sup} represented by area 2C-2R-2V.

As the expansion process in throttling devices are isenthalpic rather than isentropic, therefore, process 3-4C in Figure 1.1 would be 3-4R as shown in Figure 1.3 along the constant enthalpy line in actual system. This reduces the area of cooling capacity by an area of a-d-4R-4C and also increases the work required by an equal amount denoted as Q_{exp} and W_{exp} respectively. Therefore, isenthalpic expansion

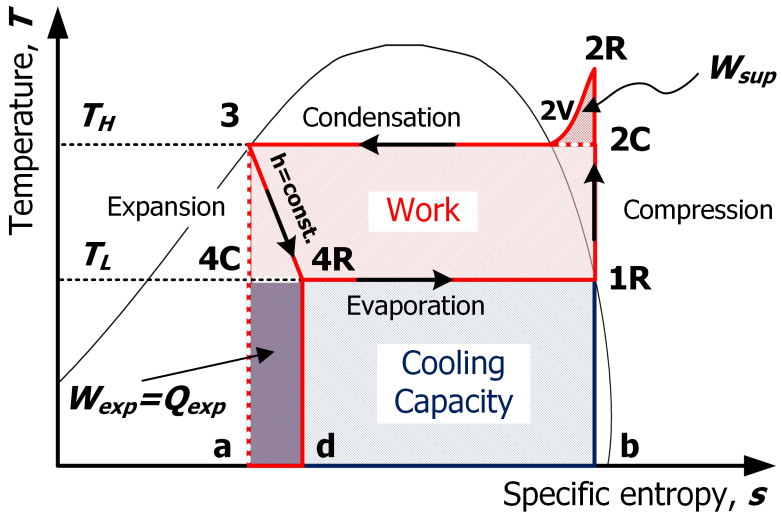

Figure 1.3: Evans-Perkins cycle $T-s$ diagram

inflicts a two-fold penalty on COP of actual cycle which is expressed as Equation 1.2.

$$COP_{act} = \frac{Q_{act} - Q_{exp}}{W_{act} + W_{exp} + W_{sup}} \tag{1.2}$$

COP reduction due to isenthalpic process in expansion valve can be reduced by many different methods. One of the simplest is internal heat exchange that reduces the generation of flash gas during expansion by introducing more subcooling at the inlet of the expansion device. However, methods that involve expansion work recovery are known to be more beneficial in terms of cycle efficiency and cooling capacity. A common feature of methods that involve work recovery is that they attempt to utilize the kinetic energy released during the pressure reduction of the fluid as it passes from the high to the low-pressure side instead of dissipating it in a throttling process. Thus, an isentropic expansion process is approached rather than isenthalpic throttling. This increases the cooling capacity, because the specific enthalpy at the evaporator inlet is reduced. Therefore, devices that can approach expansion closer to isentropic process are worth exploring.

The Ranque-Hilsch vortex tube is an unconventional expansion device which was discovered by French physics student George Ranque in 1930. The physical phenomenon was further explained by Hilsch [1] in 1947 who named the device as 'vortex tube'. As per the available literatures, it is found that vortex tube has the potential to perform better than isenthalpic expansion. The device also possesses

the advantage of being robust and cost-effective as it does not have any moving parts. However, a thorough investigation to measure the performance of existing vortex tubes operating with refrigerants is still due. Therefore, it is the aim of this thesis to experimentally and numerically investigate the capability of commercially available vortex tubes to improve the COP of the actual refrigeration cycle through incorporation of the device in the system. Special emphasis is given to identify the areas of limitation of operation with two phase refrigerant flow. Once the operating parameters are investigated and clearer understanding of the vortex tube operation is obtained, focus is shifted to numerically predict the benefits of a newly proposed refrigeration cycle utilizing vortex tube.

1.2 Structure of thesis

The document is organized in a number of different sections. Chapter 2 presents the results of a detailed literature review on prior work carried out in the area of expansion work recovery using different devices including vortex tube. Chapter 3 contains the details of the experimental study conducted to understand the performance of vortex tube. Chapter 4 introduces a novel cycle using vortex tube and contains numerical analyses carried out to assess the expected improvement in COP resulting from the incorporation of vortex tube in the conventional refrigeration cycle. Finally, a concluding summary of the major findings of this study as well as recommendations for future work are provided in Chapter 5. Appendix A contains the experimental data with air and refrigerant R134a.

CHAPTER 2

LITERATURE REVIEW

A review of the available literature is conducted to learn from previous work carried out in the field of interest. The literature search is greatly aided by the web-based browsing tool ENGINEERING VILLAGE, a service offered by Elsevier Inc. Special emphasis is placed on reviewing prior work on vortex tube application with different fluids. Also, a brief attention is provided to various other expansion work recovery devices to draw a comparison with vortex tube.

2.1 Expansion work recovery with different devices

There are devices that utilize the kinetic energy released during pressure reduction of the fluid as it passes from the high to the low-pressure side instead of dissipating it in a throttling process. Thus, an isentropic expansion process is approached rather than isenthalpic throttling. This increases the cooling capacity as the specific enthalpy at the evaporator inlet is reduced. Simultaneously, the extracted work rate can be used to reduce the power required by the compressor. Therefore, the COP of the system increases for two reasons.

Refrigerant expanders are centrifugal as well as positive displacement type including scroll, rotary vane, rolling piston and free piston devices that aim to achieve isentropic expansion. Many of these designs are built as turbo-expanders in which the expander unit shares the same drive shaft as the compressor as shown in Figure 2.1. Robinson and Groll [2] numerically investigated the contribution of different components in producing irreversibility in vapor compression refrigeration cycle using carbon dioxide as working fluid. They found that, replacing the expansion valve with an expansion work recovery turbine with an isentropic efficiency of 60% reduces the processs contribution to total cycle irreversibility by 35%.

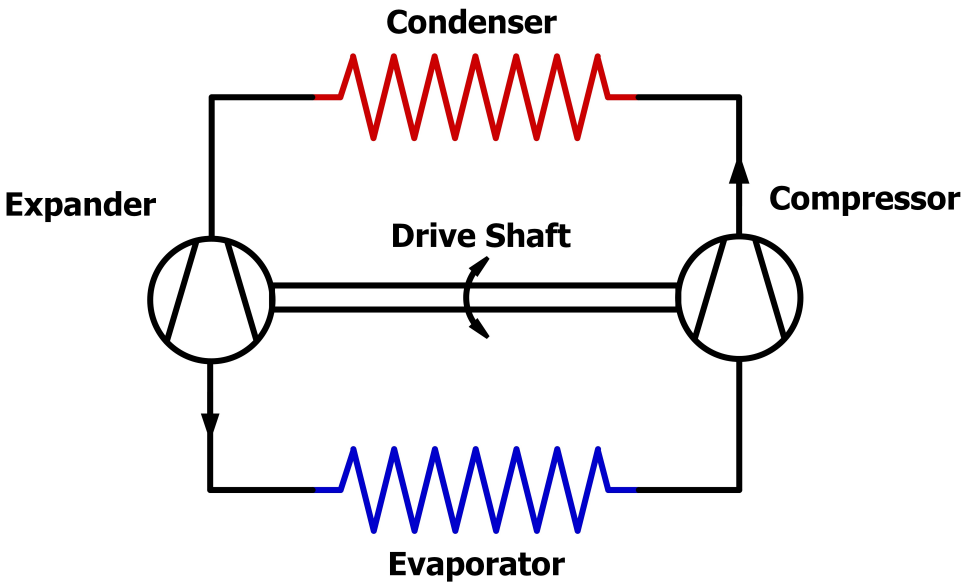

Figure 2.1: Refrigerant expander used in vapor compression refrigeration cycle

Despite having some potential to improve cycle performance, these devices, being highly integrated, can be subjected to several operational difficulties. If there is only one compressor in the system, and both the compressor and the expander are of the positive displacement type, the volumetric flow rate through the expander is fixed by its volume displacement rate since the compressor and the expander are operated on the same shaft. Another difficulty can be the heat conduction through the shared housing and shaft which can severely reduce the desired work recovery effect. One more adversity commonly encountered in centrifugal expanders is the possibility of two-phase flow damaging the equipment surfaces by erosion.

An alternative to expanders are two-phase ejectors that also aim to achieve isentropic instead of isenthalpic expansion, thereby recovering throttling losses. A schematic of a typical two-phase ejector cycle is shown in Figure 2.2

In case of this cycle being operated ideally, the saturated vapor coming from the vapor port of the liquid-vapor separator enters the compressor and is isentropically compressed to a high pressure and temperature. Heat is isobarically rejected in the condenser. In the motive nozzle at point for 4 in Figure 2.2, the single-phase motive fluid is isentropically expanded to the mixing pressure. During the expansion process, the motive fluid gains kinetic energy. Furthermore, as the fluid crosses the saturated liquid line, the refrigerant starts to flash, be-

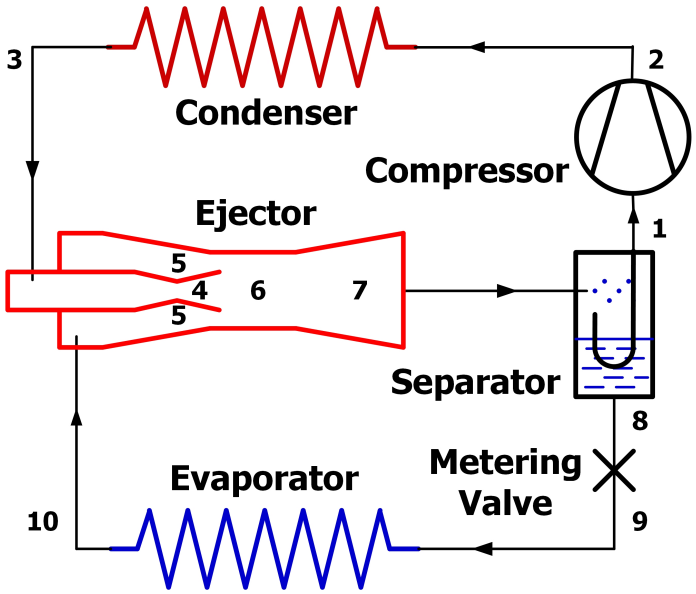

Figure 2.2: Standard two-phase ejector system layout

coming a two-phase flow. Lawrence and Elbel [3] observed that, ejector cycle with COS configuration could achieve COP improvements upwards of 10% over a conventional cycle under operating condition that slightly favor the ejector cycle. In reality however, the expansion process might occur too rapidly for the two-phase mixture to maintain hydrodynamic and thermodynamic equilibrium. Consequently, these metastability effects might cause a delayed flashing of the flow which could potentially influence the performance of the ejector.

The limitations in using the above mentioned devices pose a need to explore other promising devices and cycles that offer robust and cost effective solution to recover expansion work or waste heat to improve system performance.

2.2 Vortex tube as an expansion device

The vortex tube, shown schematically in Figure 2.3 can act to separate and incoming flow of single-phase high pressure fluid flow into two low pressure streams of different temperatures. Temperature of the fluid coming out from one of the low pressure exits can rise above that of incoming stream. While on the other low pressure exit, the fluid temperature becomes lower than that of the incoming stream. This pressure reduction and flow separation is achieved without any moving parts

which leads to its significant advantage over other devices for being robust and inexpensive.

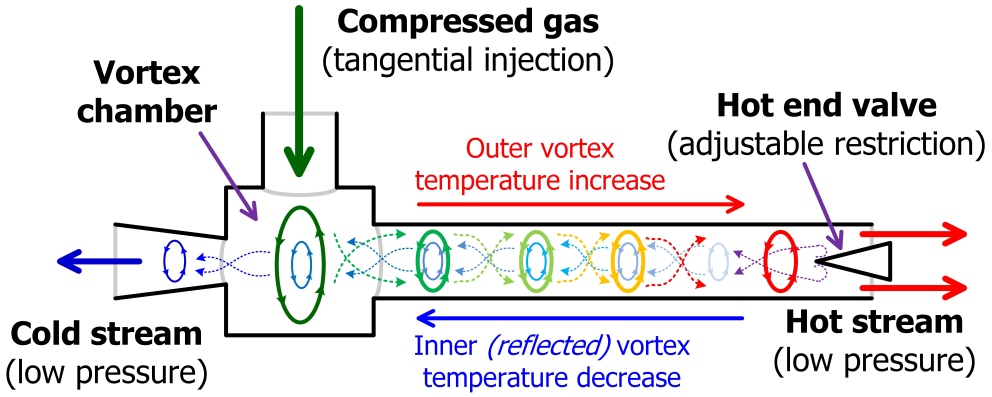

Figure 2.3: Vortex tube schematic diagram

State of the art vortex tubes have swirl generators fitted inside the vortex chamber for producing swirling fluid motion. The resulting flow acceleration that causes high rotational rates of the incoming gas. The hotter exit of the vortex tube has an adjustable valve that controls the distribution of mass between the two exits and plays important role in creating two concentric flows inside the cylinder. The swirl generator and the hot end valve are shown in Figure 2.4

Figure 2.4: Components of commercially available vortex tube

Hilsch [1] provided an explanation to the vortex tube phenomenon which is widely accepted till today. As per that explanation, fluid is flown tangentially into the vortex chamber by using tangential inlets. The swirl generator that is used in newer designs provide tangential inlet vanes that also serve the same purpose. The fluid entering tangentially through the swirl generator moves with a screw-like motion along the wall of the vortex tube. The centrifugal force and the internal friction of the gas produce a lower pressure in the axial region. Hence,

the fluid can get entrained through the cold end opening as it is closer to the vortex chamber as shown in Figure 2.3. This is avoided by throttling the flow at the hot end by attaching an adjustable valve. The valve is placed sufficiently away from the vortex chamber so that the gas reaching it loses most of its screw-like motion because of internal friction. By partially closing of the valve, it is possible to force a fraction of the fluid stream to escape through the cold end. This fraction increases with increasing internal pressure and it originates in the region near the axis of the vortex tube. The fluid escaping through the cold end is expanded in the centrifugal field from a region of high pressure near the wall of the vortex tube to a pressure in the region near the axis. The inner fluid flow transfers a considerable part of its kinetic energy by means of internal friction to the peripheral layers. It is worth mentioning here that, in the absence of internal friction, and with a sufficient pressure gradient, the velocity of the fluid would increase during expansion between the circumference and the axis of the vortex tube, acting like a free vortex. The internal friction, however, is particularly effective in this region as the two concentric vortices flowing in opposite directions are in contact with each other. The internal friction causes a flow of energy from the axis to the circumference by trying to establish a constant angular velocity throughout the cross section of the tube resembling a solid body rotation. The inner vortex loses its momentum which is imparted on the outer vortex. Therefore, a decrease in the heat content of inner fluid stream and an increase in the heat content of the outer fluid stream occurs, if the heat exchange with the surrounding though the wall of the tube is prevented. Hence, two exit streams of different temperatures are achieved.

2.3 Vortex tube studies with single and two phase fluid

This section summarizes the investigation of vortex tube behavior with different fluids. A good amount research work had been done using compressed air with the vortex tube in the early stages of development. Stephan *et al.* [4] experimented with vortex tube using compressed air with inlet pressure ranging from 150 kPa up to 500 kPa. The valve at the hot exit was adjusted to provide different mass flow distribution between the two exits. The ratio of mass flow rate going out through the cold exit and the incoming mass flow rate was denoted as the cold mass fraction as shown in Equation 2.1

$$y_c = \frac{\dot{m}_c}{\dot{m}_o} \tag{2.1}$$

It was observed in this study that with increasingly higher inlet pressure, the temperature difference between the hot and the cold outlets increased. However when the hot end valve was close to being completely shut that led to cold mass fraction being more than 0.95, the temperature difference diminished. Similar behavior was observed when the hot end valve was close to being completely open. The maximum hot end temperature observed by them was around 75°C at 500 kPa inlet pressure with hot end valve set to a condition such that, cold mass fraction was around 0.9. However, the cold side temperature at that valve setting was 5°C. As the hot end valve was gradually closed, the temperature of the hot exit decreased. However, the temperature at the cold end also dropped with the gradual closure of the hot end valve. The minimum cold exit temperature was observed when cold mass fraction was around 0.3. In this case, the cold and the hot exit fluid temperatures were observed to be -35°C and 15°C respectively. This indicates that, it is not possible to achieve the maximum hot side and minimum cold side temperatures at single setting of the hot end valve.

Aydin, Markal and Avci [5] stated that, although the vortex tube can be considered to possess certain advantages than other refrigerating or heating devices because of being simple, having no moving parts, using no electricity or chemicals and having long operation time, yet their critical disadvantage is their low thermal efficiency. They suggested the calculation of cooling efficiency of the vortex tube based on the principle of adiabatic expansion of ideal gas for single phase fluid e.g. air. Therefore, the isentropic efficiency can be written as shown in Equation 2.2. As per their investigation, the maximum isentropic efficiency of the cooling side was found to be around 45% with cold mass fraction of around 0.5 for air with inlet pressure of 300 kPa and outlets open to atmosphere.

$$\eta_{isen} = \frac{T_o - T_c}{T_o \left(1 - \left(\frac{P_o}{P_c}\right)^{\frac{k-1}{k}}\right)} \tag{2.2}$$

Wu *et al.* [6] investigated the vortex tube operation with single phase refrigerant. Using R-22 with inlet pressure of 383 kPa (T_{sat} = 8°C), they observed a

temperature drop of around 10°C at the cold outlet from the inlet refrigerant temperature. The temperature drop caused by isenthalpic throttling and isentropic expansion for the same inlet and outlet conditions obtained in the experiment are calculated as around 7°C and 53°C respectively. The observation suggested the fact that the vortex tube could achieve lower temperature at the cold outlet than what is achievable in isenthalpic throttling for similar inlet and outlet conditions.

Collins and Lovelace [7] investigated the behavior of vortex tube with two-phase propane. They observed that, the temperature separation between the hot and cold outlet was significant when the inlet quality remained above 80% extending in to the superheated region. At 80% quality, for vortex tube inlet pressure of 791 kPa (T_{sat}=31°C) and outlets being open to atmosphere, the hot and cold exit temperatures were found to be 35°C and -5°C respectively. The cold mass fraction in this case was 0.8. They hypothesized that, the possible appearance of the liquid droplet on the inner wall during vortex tube operation at lower qualities diminish the temperature separation, as cooler liquid droplets are evaporated on outer hot walls.

2.4 Numerical studies of potential vortex tube applications

In the literature, several application of vortex tube in refrigeration cycle are found. These proposed cycles are investigated numerically and show considerable potential to improve refrigeration cycle performance. However, experimental validation of these cycles is yet to be completed. Liu and Jin [8] analyzed a CO_2 transcritical two stage compression refrigeration cycle using vortex tube expansion by thermodynamics method. In their thermodynamic model, the gas expanding from gas-cooler pressure to evaporation pressure in the vortex tube is assumed to be divided into three fractions: saturated liquid, saturated vapor and superheated gas. The saturated liquid and vapor are mixed again and sent through the evaporator to provide useful cooling effect. The superheated gas is cooled in the heat exchanger and mixed with the gas coming from the evaporator before entering the compressor. The cycle is shown in Figure 2.5. The concept of this type of vortex tube is based on the design introduced by Maurer [9]. Upon comparison of the results with that of a conventional throttle cycle, the COP of the

vortex tube cycle is found to be superior. In the calculation condition of the study, COP of the vortex tube cycle improved from 2.4% to 16.8% than that of the throttle cycle. It was also observed that, with the increase of the cold mass fraction, the COP increases slightly, while performance improvement of the vortex tube cycle increases by considerable amount. However, in practical application, the existence of saturated liquid is expected to diminish the temperature separation. Also, extraction of liquid directly from the vortex tube can be highly challenging from a design perspective. These limitations make this cycle unrealistic despite its potential.

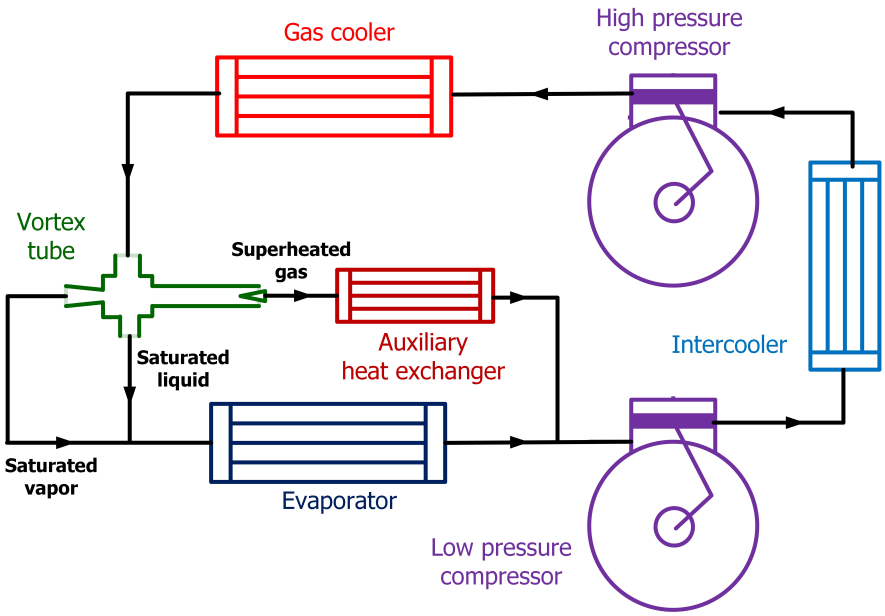

Figure 2.5: CO_2 transcritical two stage compression refrigeration cycle with vortex tube

Another application of vortex tube being used refrigeration cycle is numerically analyzed by Li *et al.* [10] where the device is used to replace the expansion valve of the transcritical carbon dioxide system as shown in Figure 2.6. According to the authors, due to Ranque-Hilsch effect, saturated CO_2 liquid at evaporation pressure leaves the cold end of the vortex tube, while superheated CO_2 vapor at evaporation pressure exits at the hot end of the vortex tube. The superheated vapor enters an auxiliary heat exchanger and dissipates heat to the environment. The cooled down CO_2 vapor stream is then mixed with the saturated liquid again entering the evaporator to extract heat from the low temperature heat source. The maximum

increase in COP using a vortex tube, assuming ideal expansion processes, was obtained about 37% compared to the one using an isenthalpic expansion process. Considering a more realistic efficiency for the vortex tube of 0.38, the increase in COP is about 20% compared to the one using an isenthalpic expansion. In order to achieve the same improvement in COP using a vortex tube. However, again in case of practical application, the existence of saturated CO_2 liquid will diminish the possibility of achieving superheated vapor at the hot end of the vortex tube. Therefore, this takes this cycle to a distant possibility of becoming realistic.

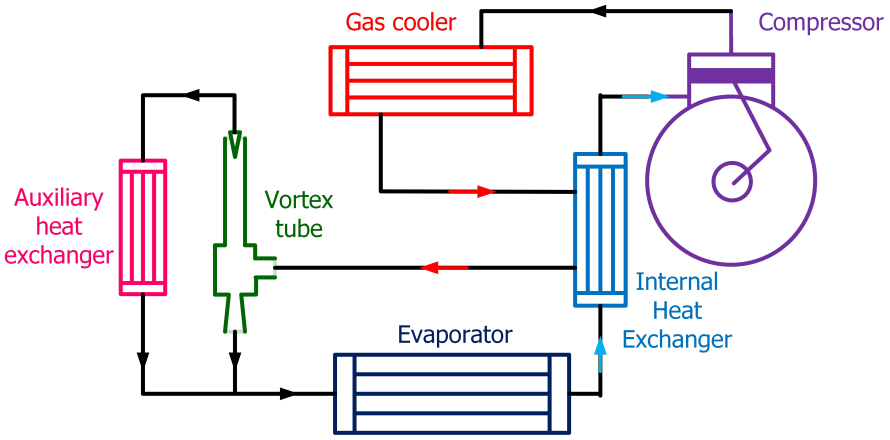

Figure 2.6: Transcritical CO_2 refrigeration cycle with vortex tube expansion device

2.5 Current applications of vortex tube

Vortex tubes are primarily used in machine shops for cooling of cutting tools (lathes and mills, both manually-operated and CNC machines) during machining. The vortex tube is well-matched to this application: machine shops generally already use compressed air, and a fast jet of cold air provides both cooling and removal of the metal chips produced during machining. Other notable applications include cooling of blow molded and welded parts. Compared to conventional refrigeration or water cooling, vortex tubes offer a number of advantages: low cost, compact design, inherent reliability and cleanliness. These attributes make vortex tubes the cost effective choice for many small part cooling operations.

The literature review done so far indicate that, the vortex tube has the potential to obtain better expansion performance than isenthalpic expansion device for refrigerants if it is operated with above 80% quality liquid-vapor mixture, saturated and superheated vapor. However, this capability is yet to be explored by designing proper refrigeration cycle. Therefore, exploring the performance of commercially available vortex tubes with refrigerants is necessary. Based on the performance of vortex tube with refrigerants, realistic refrigeration cycles can be proposed and numerically analyzed to estimate overall gain in system COP and capacity.

CHAPTER 3

EXPERIMENTAL STUDY OF VORTEX TUBE

The main features of the experimental equipment are presented in this chapter. The vortex tube and other components making up the experimental vortex tube performance testing facility are described in detail. Furthermore, this chapter contains a description of experimental procedures employed for typical test of vortex tube performance and discusses the results obtained.

3.1 Performance evaluation of vortex tube using air as working fluid

In this section, the major features of the experimental facility developed for testing with air are described. Discussion of experimental results and evaluation of performance parameters are also provided. The objective is to compare the performance characteristics of the vortex tube used in this research with experimental findings obtained by Stephan *et al.* [4].

3.1.1 Vortex tube

The vortex tube used in this research is commercially manufactured by EXAIR. This particular vortex tube belongs to the 3200 model series. The length of the vortex tube is measured as 0.105 m. The vortex tube is rated at 786 kPa. The components of the vortex tube are shown schematically in Figure 3.1. The vortex tube can produce a number of flow rates as determined by the internal plastic part called the swirl generator. For the vortex tube used in this study, there are three swirl generators available with the vortex tube namely the 2R, 4R and 8R. The number indicates the maximum capacity (SCFM of air consumption) with that particular generator installed inside the vortex tube. The letter 'R' stands for maximum refrigeration. The 'R' type generators are used for most applications

where complete heat exchange is desired e.g. part cooling, enclosure cooling. One other type of generator is also available which is called the 'C' type that provides maximum cold temperature. In this study, the 'R' type generators have been used to investigate the refrigeration effect that the vortex tube can provide when used with air and refrigerant.

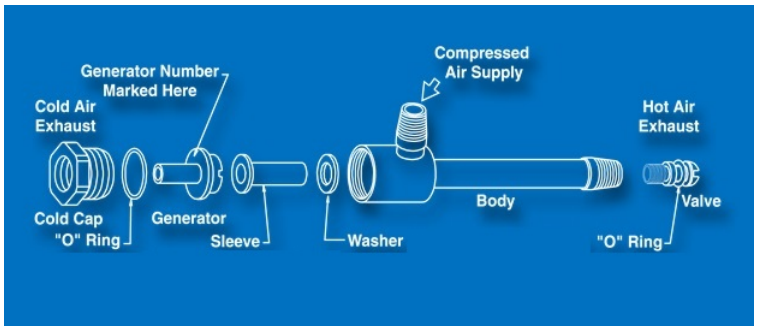

Figure 3.1: Components of EXAIR 3200 series vortex tube

3.1.2 Experimental setup layout

The vortex tube described in the previous section is installed in the laboratory to experimentally investigate the temperature separation performance. A schematic diagram of the experimental setup is shown in Figure 3.2. The laboratory facility is shown in Figure 3.3.

As shown in Figure 3.2, the vortex tube is mounted vertically with the hot end facing upwards. By installing a T-joint at the hot end, provision is made to adjust the hot end valve with a screwdriver. Compressed air supply available from building facility is supplied to the vortex tube inlet. A valve is used to throttle the compressed air and thereby control the inlet air pressure. The inlet pressure also dictates the amount of inlet mass flow. The hot outlet of the vortex tube is controlled with the hot air exhaust valve which determines the amount of flow allowed to exit through the hot outlet. During the vortex tube operation, the opening of the hot end can be controlled by adjusting the hot air exhaust valve using a screwdriver. The hot and the cold outlets are kept open to the atmosphere. Mass flow meters, pressure transducers and thermocouples are intalled at the inlet and the two outlets for measurement. The vortex tube inlet mass flow rate is determined by using a Coriolis type mass flow meter. The two outlet air mass flow rates of

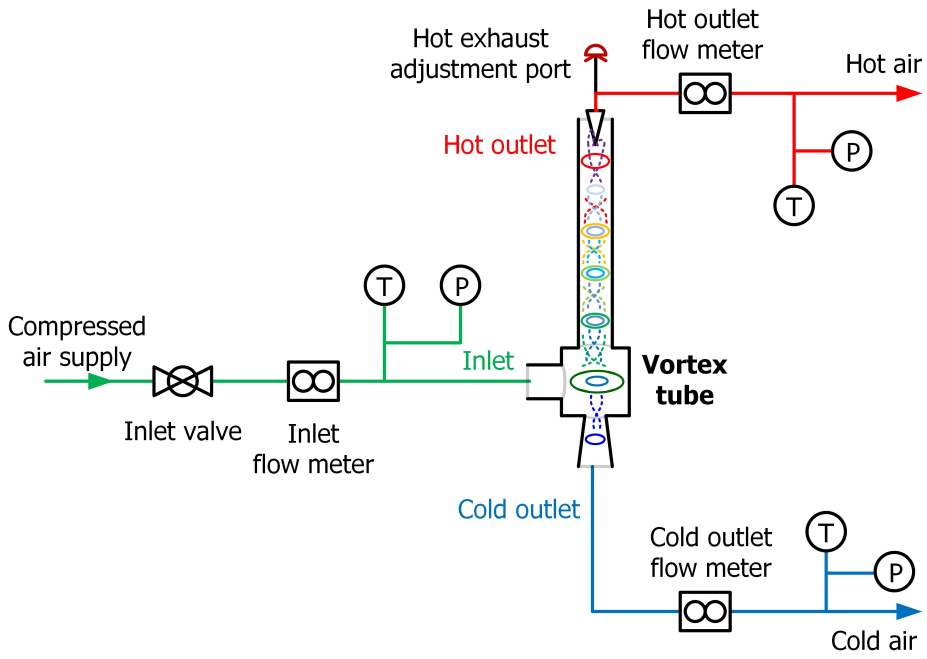

Figure 3.2: Schematic diagram of vortex tube performance test facility using air as working fluid

the vortex tube are determined with hot wire anemometer type sensors. The temperature readings are obtained from ungrounded T-type immersion thermocouple probes to reduce effects by electromagnetic noise. Piezo-electric transducers are used to read absolute pressures. The details of the instruments used to obtain the experimental measurements of the test facility are summarized in Table 3.1.

3.1.3 Test methodology

At the beginning of the each test, a vortex generator from the available 2R, 4R and 8R size is chosen. By turn, all the three sizes are fitted and tested. The total assembly is pressure tested by connecting the inlet to a nitrogen cylinder and capping the two outlets. The system is pressurized to approximately 600 kPa. After charging the system with nitrogen, the inlet valve is closed and the pressure is continuously monitored. If the pressure is observed to be decreasing over the time, then leaks are detected by spraying soapy water onto every compression fitting and checking if there is any bubble formation. The leaking compression fittings are then tightened further. Consistent monitoring of the pressure data using the data acquisition system is continued to find out if there is any change in the

Figure 3.3: Experimental setup for vortex tube performance test using air as working fluid

system pressure. Leak testing is carried on until the pressure inside the system stops decreasing. It is important to mention here that, as pressure recordings are used to determine leaks, a single-phase vapor has to be charged to the system, because leaks cannot be detected by pressure drops using a two-phase fluid. Once the leak test is complete, the system is discharged.

The testing of vortex tube with a certain swirl generator is initiated by starting the data acquisition system and then gradually opening the inlet valve to let compressed air flow through the system. Inlet pressure is controlled using the inlet valve. In the beginning, the adjustable hot air exhaust valve is kept at fully open position. The hot air exhaust valve is then adjusted to different settings to change the cold mass fraction and observe variation of temperature separation. Before recording the pressure, temperature and mass flow rate data at the inlet and the two outlets for a set inlet pressure, a time of approximately ten minute is allowed to elapse in order to achieve steady state. Once the data has been recorded for different cold mass fractions at a particular inlet pressure, the inlet valve setting is set at a different position to set different inlet pressure and the experiment is repeated.

Table 3.1: Measurement uncertainties of instruments used to investigate vortex tube performance with air as working fluid

Sensor	Range	Unit	Accuracy
Type-T thermocouples	-200 to 200	°C	±0.5 absolute
Absolute pressure transducer (vortex tube inlet)	0 to 1724	kPa	±0.13% full scale
Absolute pressure transducer (vortex tube hot outlet)	0 to 689	kPa	±0.13% full scale
Absolute pressure transducer (vortex tube cold outlet)	0 to 689	kPa	±0.11% full scale
Coriolis type mass flow meter (vortex tube inlet)	0 to 0.19	kg/s	±0.15% reading
Hot wire anemometer type mass flow meter (vortex tube hot outlet)	0 to 0.01	m^3/s	±1% full scale

Repeatability of the experimental results is confirmed by running certain data points at identical test conditions for repeated times. Consistently good agreement between the results of the similar test conditions taken at different times is observed with a deviation of ±1.5°C between values recorded in repetitive test.

3.1.4 Data acquisition

All experimental data are recorded with a HEWLETT-PACKARD 75000 data acquisition system. Every six seconds, a voltmeter module in combination with four multiplexer cards reads 64 channels. Two of the multiplexer cards are equipped with thermistors allowing to directly interpret the thermocouple signals as temperature readings. AGILENTVEE data acquisition software is used to monitor the relevant data online. A sample screenshot of the program is shown in Figure 3.4. More details regarding the data acquisition system can be found in the description of an earlier study carried out in the same laboratory by Elbel [11].

3.1.5 Experimental uncertainties for vortex tube performance test with air

Uncertainty propagation is performed using EES (2013). The determined values of uncertainty for the experimental performance parameters reported for vor-

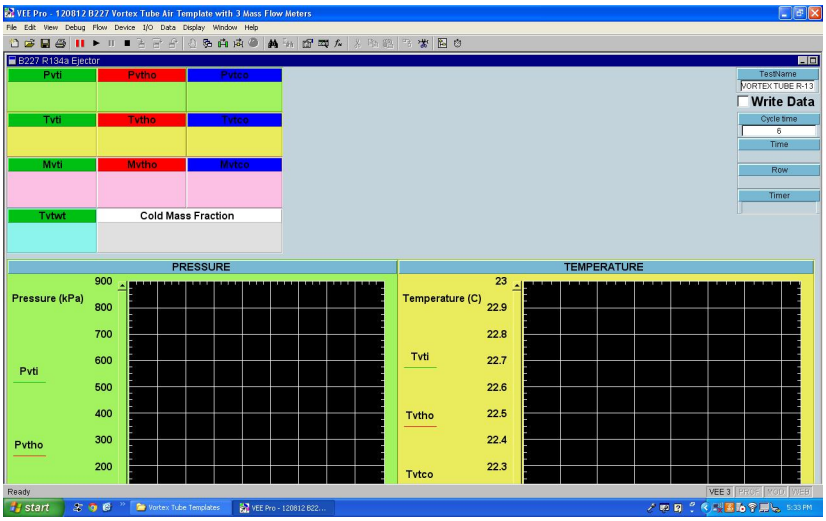

Figure 3.4: Screenshot of the data acquisition software interface

tex tube experiments with air are shown in Table 3.2.

Table 3.2: Experimental uncertainties of variables reported for vortex tube experiments with air as working fluid

Variable	**Absolute uncertainty**
y_c	± 0.004
$\eta_{c,isen}$	± 0.003
Q_c	± 0.009
Q_h	± 0.008

3.1.6 Experimental results of vortex tube performance with air

This section contains experimental vortex tube performance results using air as working fluid. Important operational parameters such as the inlet pressure and cold mass fraction are varied and temperature separation between the two outlets are observed. Based on the collected data, other performance characteristics such as the isentropic efficiency, cooling capacity of the cold side and heating capacity of the hot side are also calculated.

The variation in temperature separation with respect to different cold mass fractions for the 2R generator shown in Figure 3.5. The experiments are carried out for three different inlet pressures of 400, 600 and 780 kPa. The results show that

a maximum hot end temperature of around 70°C is achieved at cold mass fraction of roundabout 0.83. On the other side, minimum cold side temperature of around -10°C is obtained at cold mass fraction of approximately 0.4.

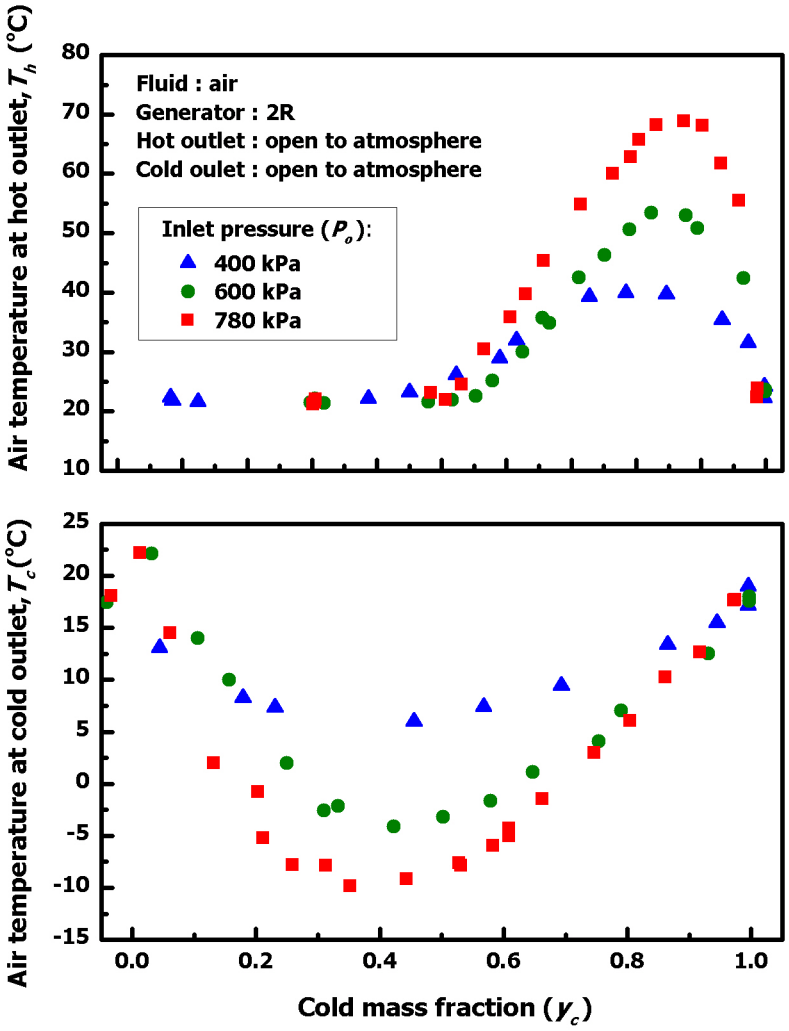

Figure 3.5: Temperature separation between cold and hot outlets using 2R generator

The discharge air temperatures from the two vortex tube outlets while using the 4R generator are given in Figure 3.6. The results show similar trends as that from the 2R generator. However, the hot side temperature gained even higher value in this case than the previous one for similar inlet pressure. For example, for a cold mass fraction of approximately 0.85 and inlet pressure of around 600 kPa, the hot side temperature is around 65°C using the 4R generator compared to 55°C obtained using 2R generator.

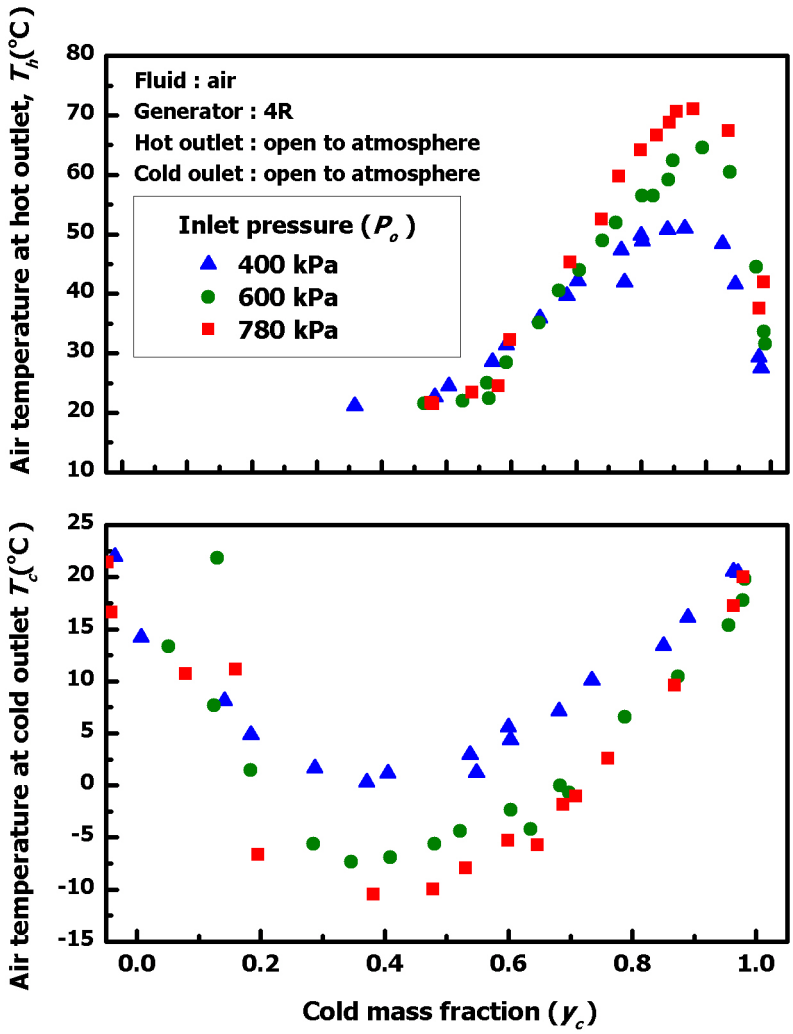

Figure 3.6: Temperature separation between cold and hot outlets using 4R generator

Temperature separation using 8R generator is shown in Figure 3.7. The data points provide a reasonable conclusion that the behavior is similar to that of other vortex generators. However, hot end temperature of around 90°C can be achieved using this generator which is considerably higher than what was achieved with other generators.

The mass flow rate for all the generators increased with the increment of inlet pressure. Figure 3.8 shows comparison of mass flow rates for the three generators operating at different inlet pressure for a fully open hot air exhaust valve. The inlet air temperature for each case is around 23°C. The difference in mass flow rate between the three generators increase as the inlet pressure increases.

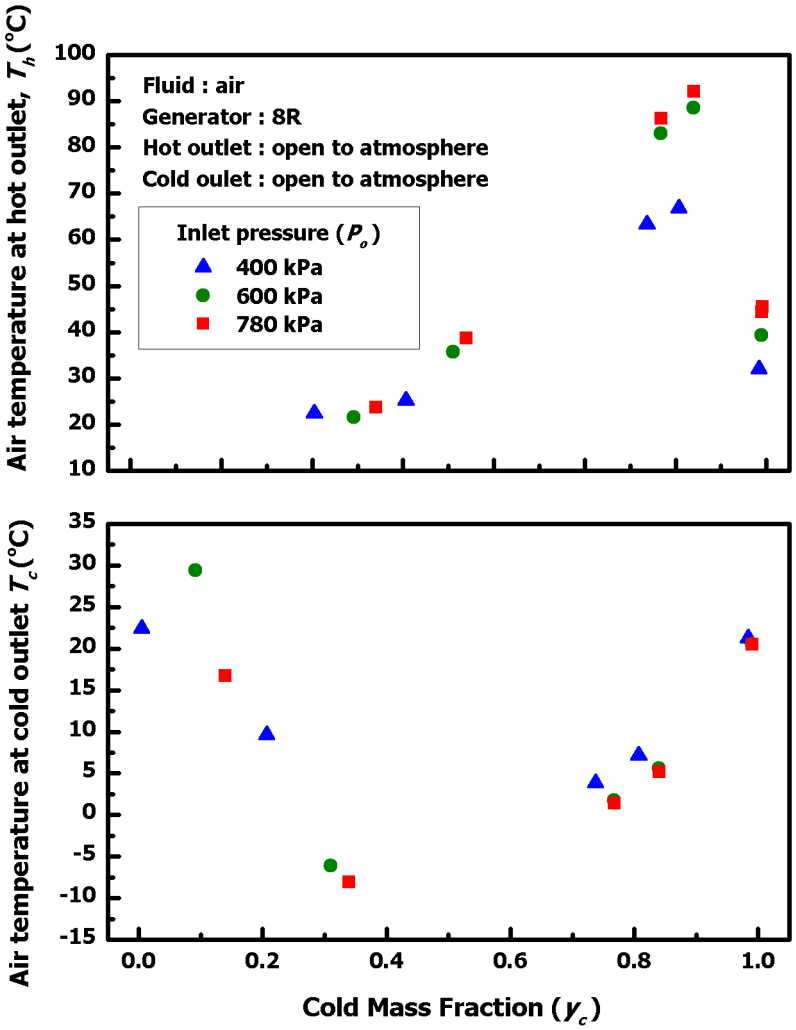

Figure 3.7: Temperature separation between cold and hot outlets using 8R generator

The results from the experiments can be interpreted as to support the findings by Stephan *et al.* [4] regarding the maximum hot end temperature at higher cold mass fractions between 0.8 to 0.9 and minimum cold end temperature at lower cold mass fractions around 0.35 to 0.45. This implies that, the extreme temperatures are not available at the same cold mass fraction. Also, the higher pressure difference between the inlet and the outlets leads to more extreme temperatures.

Based on the temperature separation data obtained from the experiment, isentropic efficiency of the vortex tube can be calculated using Equation 2.2 assuming air to behave like an ideal gas. Also, the temperature separation data showing similar trend for all the three vortex generators provide the ground to believe

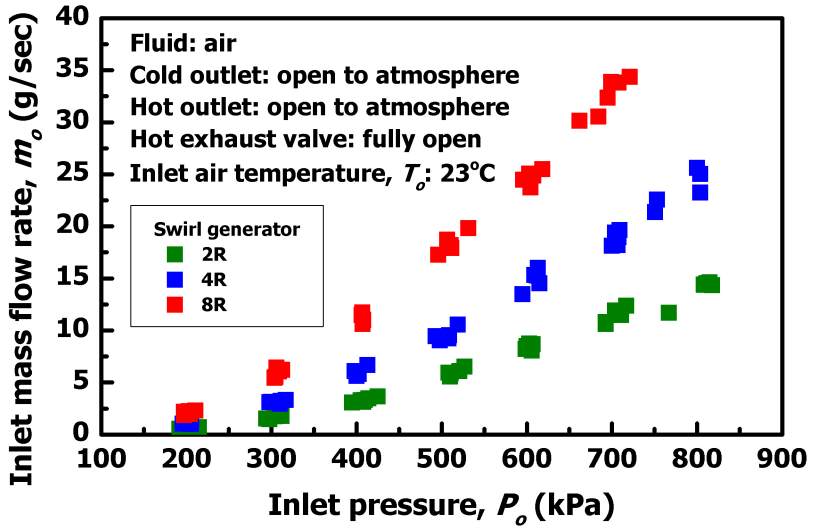

Figure 3.8: Comparison of air flow rate using 2R, 4R and 8R swirl generators at different inlet pressures

that isentropic efficiency and cooling capacity calculated from experimental data would also show similar trends. Figure 3.9 shows the isentropic efficiency for the 4R generator. The maximum isentropic efficiency achieved is around 0.15 for cold mass fraction of 0.5 for inlet pressure of 780 kPa. Also, the peak efficiency value for inlet pressure of 400 kPa is around 0.12 which indicates that, the increment of efficiency for higher inlet pressures is subtle.

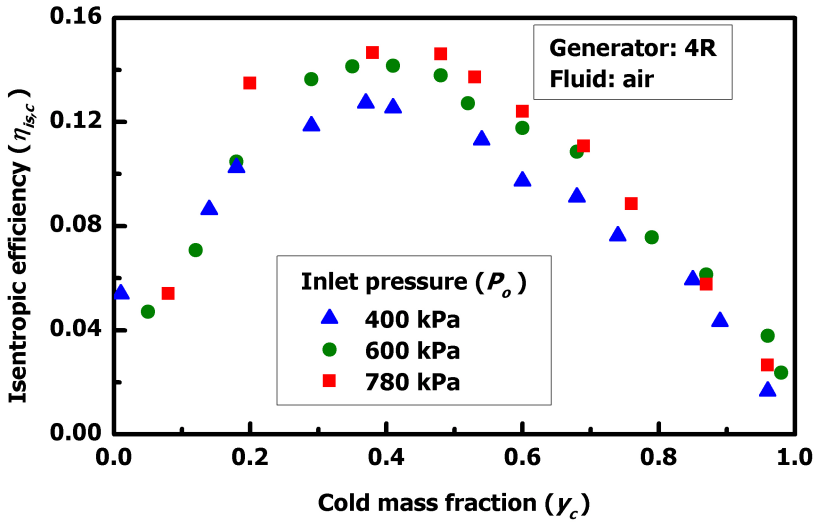

Figure 3.9: Isentropic efficiency of cold outlet considering air as ideal gas

The cooling capacity of the cold discharge can be determined by using Equation 3.1.

$$\dot{Q}_c = y_c \cdot \dot{m}_o \cdot C_p \cdot (T_o - T_c) \tag{3.1}$$

The cooling capacity of the vortex tube at different cold mass fractions using the 4R generator is shown in Figure 3.10. The capacity increases with the increase of pressure difference between the inlet and the outlet. Also, the capacity reaches its peak value of 0.36 kW for cold mass fraction in the region of 0.6 and inlet pressure of 780 kPa.

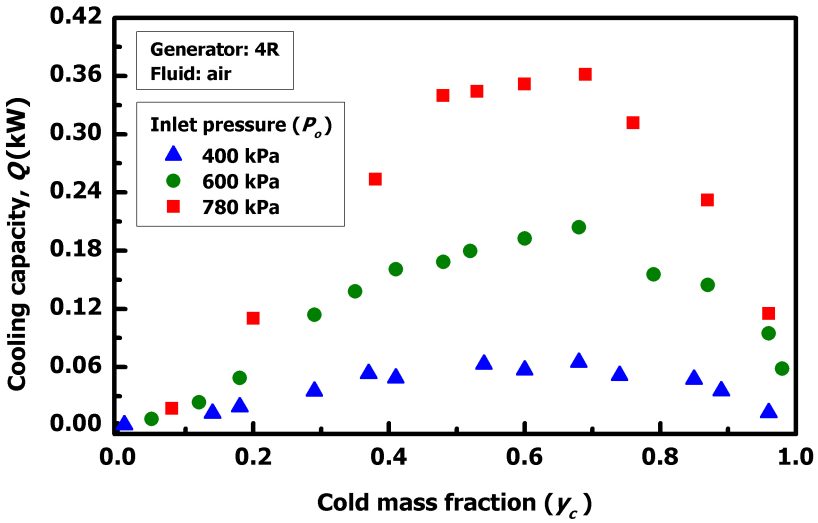

Figure 3.10: Cooling capacity of vortex tube cold discharge using 4R generator

The heating capacity of the hot discharge can be determined using Equation 3.2

$$\dot{Q}_h = (1 - y_c) \cdot \dot{m}_o \cdot C_p \cdot (T_h - T_o) \tag{3.2}$$

The heating capacity of the vortex tube at different cold mass fractions using the 4R generator is shown in Figure 3.11. Like the cooling capacity, the heating capacity also increases with the increase of pressure difference between the inlet and the outlet. The heating capacity reaches its peak value of 0.36 kW for cold mass fraction of 0.5 at inlet pressure of 780 kPa. Therefore, the cooling and the heating capacities are reaching their peak values in the region of cold mass fraction values of 0.5 to 0.6

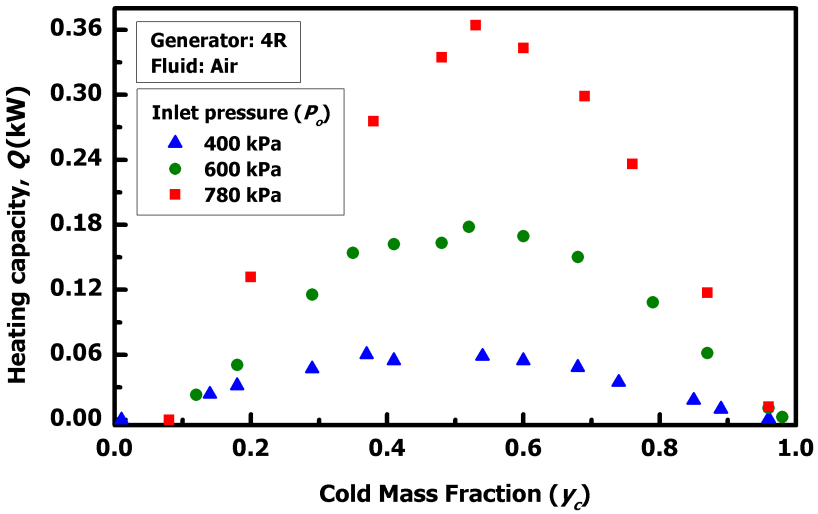

Figure 3.11: Heating capacity of vortex tube cold discharge using 4R generator

3.2 Performance evaluation of vortex tube using refrigerant R134a as working fluid

In this section, the major features of the experimental facility developed for testing with refrigerant R134a are described. Discussion of experimental results and evaluation of performance parameters are also provided. The objective is to identify areas of limitation in operation with refrigerant and study relevant operating parameters. Based on suitable operating conditions, development of suitable applications for refrigeration will be suggested in later chapters.

3.2.1 Experimental setup and its components

The vortex tube that is used in experiments with air is also used in experiments with R134a. In order to ensure a constant supply of refrigerant at desired thermodynamic condition at the inlet of the vortex tube, the system needs to be closed. In the closed system, the refrigerant is pressurized and heated to attain desired pressure, temperature and quality before being supplied to the vortex tube inlet. The cold and hot discharge from the vortex tube are collected and cooled properly to be pressurized and heated again to be supplied back into the vortex tube. To pressurize the liquid refrigerant, a reciprocating pump is used. The pressurized liquid refrigerant is then passed through a heat exchanger acting as an evaporator to raise the refrigerant enthalpy. Hot water is supplied to the heat exchanger from a tank

with an immersion heater and a submersible pump. Refrigerant at desired temperature and pressure is then supplied to the vortex tube. Temperature separation between the hot and the cold sides are measured. Discharged refrigerant from the outlets are collected and supplied in to a condenser and then passed through a receiver and then through a subcooler. The receiver separates any refrigerant vapor present after the condenser and allows only liquid to pass in to the subcooler. Both the condenser and the subcooler are heat exchangers running chilled water supply to remove heat from the refrigerant and liquefy it. The liquid refrigerant is again supplied to the pump inlet. Chilled water supply enters the subcooler first and then passes onto the condenser which makes both of those heat exchangers at a counter flow arrangement with the refrigerant. A bypass line is fitted at the pump outlet connecting it to the pump inlet through copper tubing and a valve. The bypass is used to adjust the flow of refrigerant to the vortex tube. Coriolis-type mass flow meters are used; one at the pump outlet and another at the hot outlet of vortex tube as in these two sections, the refrigerant flow will be single phase. Similar to the previous experimental setup built for testing with air, the temperature readings are obtained from ungrounded T-type immersion thermocouple and piezo-electric transducers are used to read absolute pressures. Sight glasses are installed at various locations of the system to monitor refrigerant flow.

The accuracies of the instruments used to obtain experimental measurements for vortex tube testing with refrigerant are summarized in Table 3.3

Table 3.3: Measurement uncertainties of experimental instruments used to investigate vortex tube performance with refrigerant R134a as working fluid

Sensor	**Range**	**Unit**	**Accuracy**
Type-T thermocouples	-200 to 200	°C	±0.5 absolute
Absolute pressure transducer (vortex tube inlet)	0 to 1724	kPa	±0.13% full scale
Absolute pressure transducer (vortex tube hot outlet)	0 to 689	kPa	±0.13% full scale
Absolute pressure transducer (vortex tube cold outlet)	0 to 689	kPa	±0.11% full scale
Coriolis type mass flow meter (vortex tube inlet)	0 to 0.188	kg/s	±0.15% reading
Coriolis type mass flow meter (vortex tube hot outlet)	0 to 0.038	kg/s	±1% full scale

A schematic diagram of the experimental setup is provided in Figure 3.12 followed by detailed description of the major components.

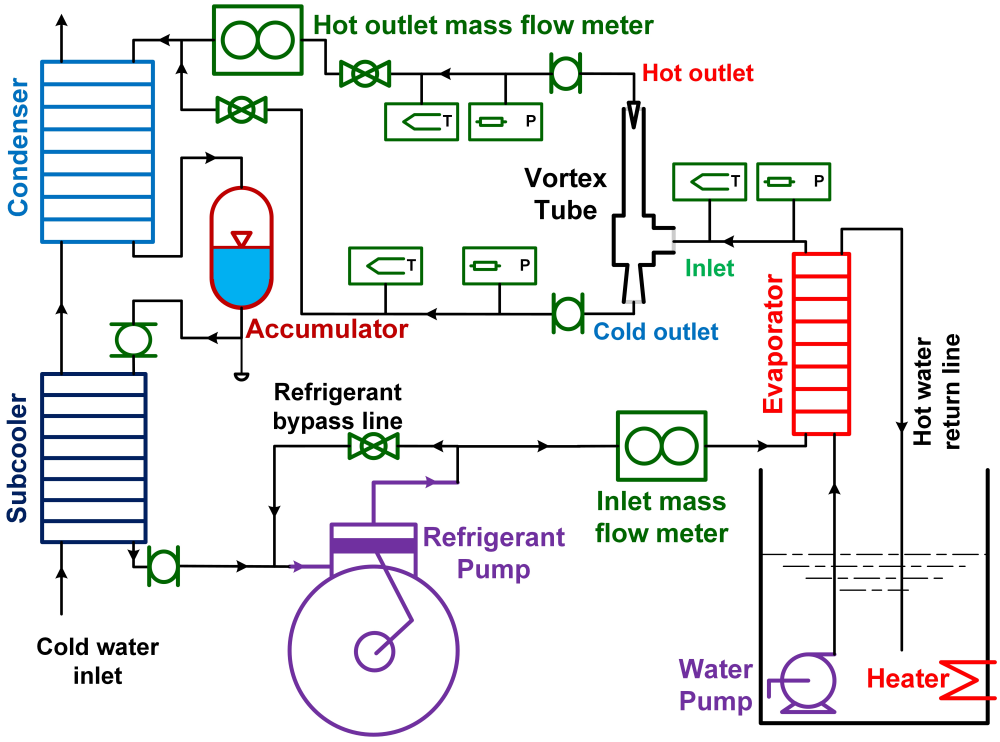

Figure 3.12: Schematic diagram of the vortex tube performance test setup using refrigerant as working fluid

Refrigerant pump

A reciprocating piston pump shown in Figure 3.13 that has three pistons and maximum flow rate of 0.0001133 m^3/s. The maximum rpm is 1750. Maximum inlet pressure that the pump can withstand is 1730 kPa. The pump can pressurize fluid up to 8300 kPa as it has a stainless steel head. Also, the pump can withstand hot fluid having temperature up to 120°C. A safety valve with pressure rating of 2758 kPa is installed close to pump outlet.

A three phase 0.6 kW electric motor is used to run the pump. The motor can rotate at maximum of 1725 rpm and is connected to a three-phase power supply of 208 V at 60 Hz. In order to control the pump speed, an adjustable frequency solid state AC drive as shown in Figure 3.14 is used.

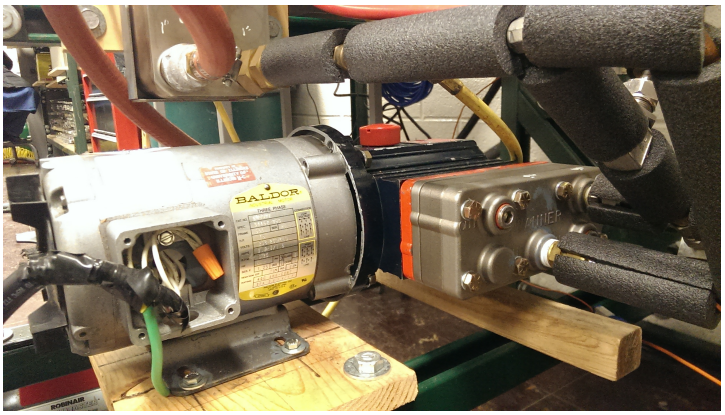

Figure 3.13: Reciprocating pump for pressurizing refrigerant

Evaporator and accessories

A brazed plate heat exchanger is used as an evaporator as shown in Figure 3.15. The heat exchanger has 30 steel plates. The heat exchanger can withstand fluid pressure and temperature up to 3100 kPa and 185°C respectively. The internal volume of the primary fluid side is around 0.00057 m^3 while that of the secondary fluid is around 0.00062 m^3. Hot water at desired temperature is supplied to the heat exchanger using a 4.5 kW immersion heater fitted in a steel tank. A submersible pump with a flow rate of 0.0033 kg/s is used to circulate hot water through the evaporator. The pump and the heater are shown in Figure 3.16.

The heater is controlled by using a PID controller along with a solid state heater controller. The PID controller takes in temperature data from a thermocouple immersed in the water tank. Depending on the water temperature, the PID controller sends signal to the solid state heater controller. Single phase power supply is connected to the solid state controller via a temperature cut-out switch operated contactor. As a safety feature for the heater, the temperature cut-out switch is used that monitors the temperature of the heater surface through a thermocouple clamped to the heater surface. The switch cuts power supply to the solid state heater controller using the contactor if the heater surface temperature rises above 95°C to prevent heater burnout. The PID controller, temperature cut-out switch as well as the solid state heater controller is shown in Figures 3.17, 3.18 and 3.19 respectively.

Figure 3.14: Variable frequency solid state AC motor drive

Condenser and subcooler

Two identical brazed plate heat exchangers are used as a condenser and a subcooler. One of the heat exchangers is shown in Figure 3.20. The maximum pressure the heat exchangers can withstand is 3000 kPa. Temperature rating of these heat exchangers is -160°C to 255°C.

Receiver

A receiver as shown in Figure 3.21, is used to force the condenser to exit saturated liquid in steady state. From the receiver, only liquid is allowed to pass on to the subcooler. The receiver is set at a height in between the condenser and the subcooler with the condenser being at the topmost position. Therefore, saturated liquid from the condenser would flow into the subcooler. A sight glass is installed after the receiver to check the presence of any vapor.

Figure 3.15: Refrigerant evaporator

3.2.2 Experimental setup layout, test methodology and data acquisition

Figure 3.22 shows the completed experimental setup. The data acquisition system and its accessories are positioned at the top of the setup. All the power supply components are attached on the right side of the setup. This is done to keep the electrical and electronic components at a distance from components using hot and cold water to avoid damage in case of water spill. At the beginning of the experiment, the data acquisition device is turned on to monitor pressure and temperature at different locations of the system. The setup is leak tested with nitrogen and soap bubble following the same procedure as described in § 3.1.3. Upon completion of the leak testing, the nitrogen gas is discharge through the charging/discharging port. A vacuum pump is used to evacuate the system. Liquid R134a refrigerant is charged into the system through the charging port. The amount of refrigerant charged is approximately 3 kg. After the refrigerant has been charged, the chilled water supply to the condenser and subcooler is turned on. Also, the hot water supply to the evaporator is started. The pump is then started at low speed. If mass flow does not increase, then 50 to 100 g of refrigerant is added by opening the refrigerant port to provide more liquid to the pump and help it start. Once the pump

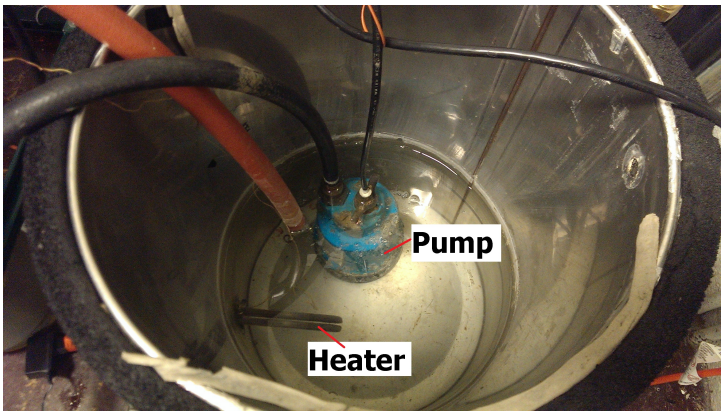

Figure 3.16: Water heater with submersible pump

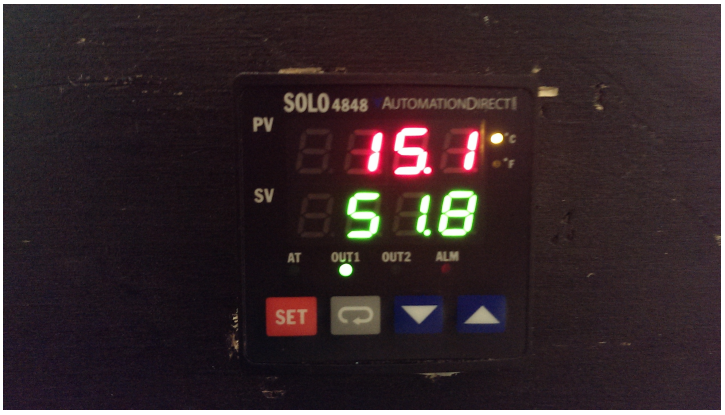

Figure 3.17: PID controller

starts to push the liquid along, speed of the pump and if needed, the bypass valve are adjusted to achieve maximum steady flow through the vortex tube. As the evaporator water temperature rises to the desired level, consistant adjustment of pump speed and monitoring of system pressure and temperature is required. Once steady operation is reached, an external valve as shown in Figure 3.23, is adjusted to different cold mass fraction. To prevent refrigerant leakage, the hot end valve fitted in the vortex tube is not accessed and is kept fully open. Instead, the external valve is used to control mass flow out of the hot side. All experimental data is recorded with an AGILENT 34970a data acquisition system. Every two seconds, a voltmeter module in combination with single multiplexer card can read up to 20 channels. The multiplexer card is equipped with and internal reference junction allowing to directly interpret the thermocouple signals as temperature readings. LABVIEW graphical programming software is used to monitor the relevant data. A sample screenshot of the data acquisition interface is provided in Figure 3.24.

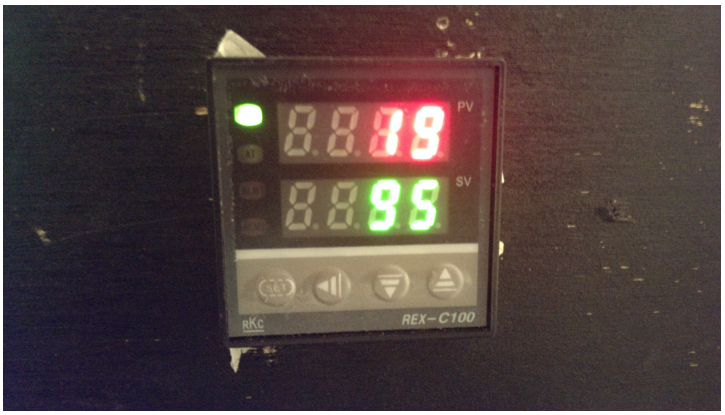

Figure 3.18: Temperature cut-out

Figure 3.19: Solid state heater controller

3.2.3 Experimental uncertainties for vortex tube performance test with refrigerant

The determined values of uncertainty for the experimental performance parameters reported for vortex tube experiments with refrigerant R134a are shown in Table 3.4. The uncertainty values are calculated using EES (2013).

3.2.4 Experimental results of vortex tube performance with refrigerant R134a

This section contains experimental vortex tube performance results using refrigerant R134a as working fluid. Important operational pressures are inlet and outlet pressures and the cold mass fraction. As the system is closed, the inlet side

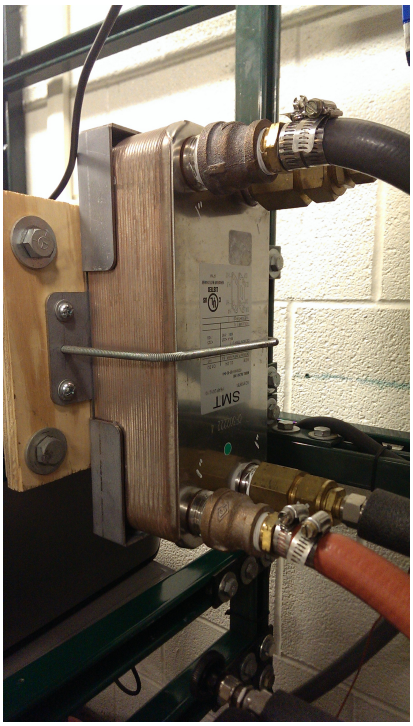

Figure 3.20: Brazed plate heat exchanger used as a condenser and a subcooler

Table 3.4: Experimental uncertainties of variables reported for vortex tube experiments with R134a as working fluid

Variable	**Absolute uncertainty**
y_c	± 0.0012
$\eta_{c,isen}$	± 0.025
Q_c	± 0.002

pressure depends on the evaporator water temperature. Also the discharge side pressure depends on the subcooled liquid temperature. Depending on the pressure difference between the inlet and the outlet, temperature separation is observed at different cold mass fractions.

2R generator

Temperature separation at the hot and cold discharge for R134a using 2R generator is investigated at different saturated inlet conditions. From the experimental results with air, it is evident that the vortex tube provides better temperature separation at higher pressure differences. In case of experiments with air, the outlets

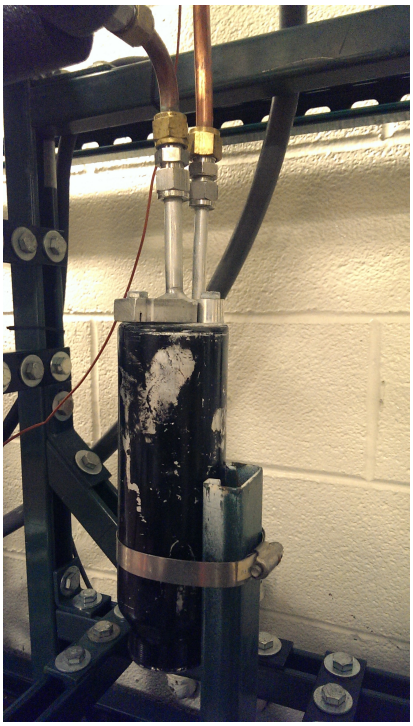

Figure 3.21: Receiver for separating refrigerant vapor

are kept open to atmosphere and vortex tube is operated at different inlet pressure with maximum of 780 kPa. This creates a pressure difference of around 700 kPa between the inlet and the outlets for operation with air. In experiments with R134a, the lower side pressure is largely dictated by the chilled water temperature. Therefore, the pressure at the discharge side is four to five times atmospheric pressure. To create pressure difference of around 700 kPa for experiments with refrigerant, the inlet pressure had to be around 1200 kPa. The inlet pressure is raised by heating the refrigerant using the evaporator before the vortex tube inlet. Figure 3.25, 3.26 and 3.27 show pressure and temperature of hot and cold outlets at different inlet pressure.

From the experimental results, it is noticeable that the hot side temperature is not observed to rise above the inlet temperature. This is different from the experimental results with air as working fluid, as the hot side temperature rises above inlet temperature in case of operation with air. This phenomenon can be attributed to the possible existence of liquid droplets of refrigerant inside the vortex tube. At cold mass fraction less than 0.4, the temperature separation decreases. Also, at cold mass fraction lower than 0.6, a pressure difference occurs between the cold

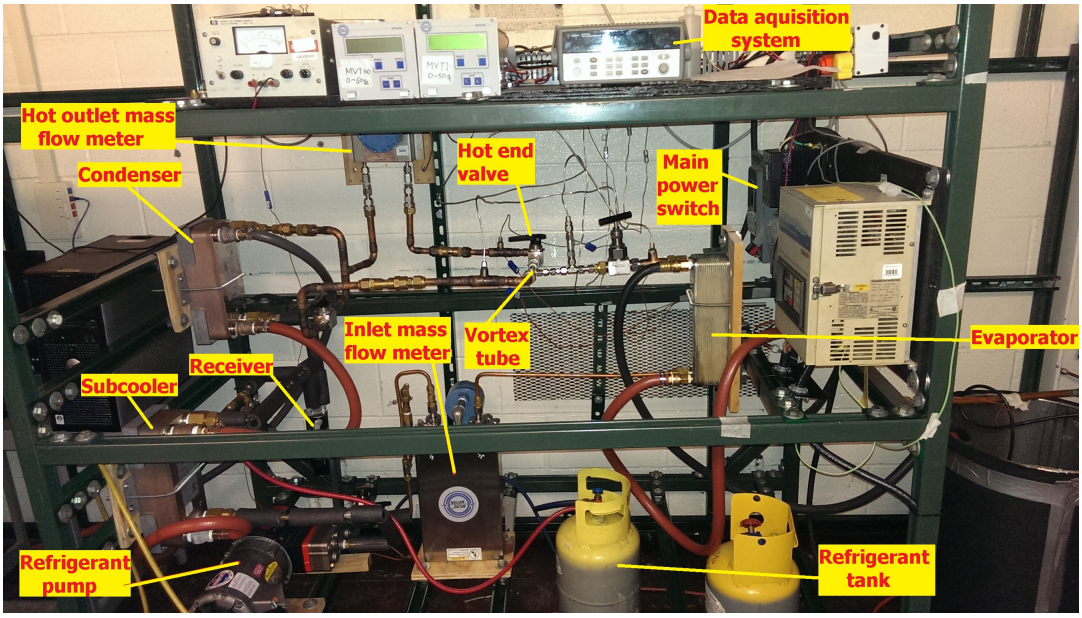

Figure 3.22: Completed experimental setup for testing vortex tube performance with refrigerant (R134a)

and the hot outlet. The pressure difference diminishes as the cold mass fraction rises close to 0.8, i.e. the hot end is gradually closed. The temperature difference between the cold and the hot side increases with the increase of cold mass fraction and inlet pressure. The maximum temperature difference between the outlets is observed around 12°C for inlet pressure of 1304 kPa. The mass flow rate through the vortex tube increases from 3.14 g/s to 4.2 g/s as the inlet pressure rises from 1015 kPa to 1304 kPa. As the inlet pressure increases, both the outlet pressures are observed to decrease. When the inlet pressure is around 1015 kPa, the outlet pressures are well above 460 kPa. As the inlet pressure increased to 1304 kPa, both the outlet pressures are below 440 kPa. Also, the temperature separation is higher as the inlet pressure increases. Therefore, the vortex tube provides better expansion resulting in higher temperature separation as the inlet pressure increases.

4R generator

Experimental results for vortex tube performance with 4R generator at different inlet conditions are provided in Figure 3.28, 3.29 and 3.30. The temperature separation in this case follows the trend observed in experiments with air up to the point that minimum cold outlet and maximum hot outlet temperatures are achieved at around cold mass fraction of 0.4 and 0.8 respectively. The mass flow

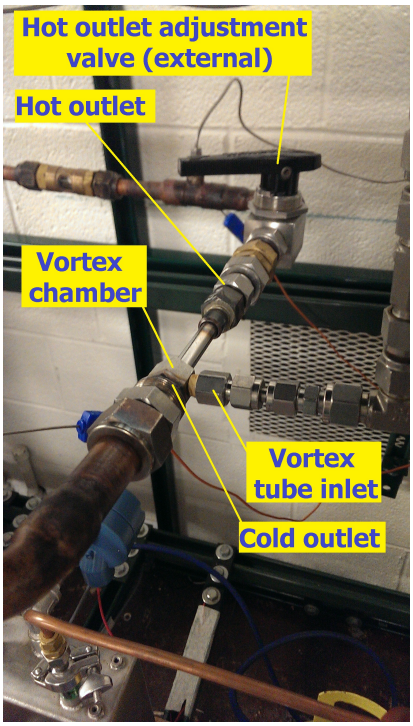

Figure 3.23: Vortex tube installed in the experimental setup

rate here also increases with the inlet pressure. The two outlet pressures have a difference of more than 80 kPa for cold mass fractions around 0.2. However, the difference diminishes at cold mass fractions of approximately 0.8. The mass flow rate decreases with the increment of cold mass fraction due to closure of the hot outlet valve. The maximum temperature separation is observed to be around cold mass fraction of 0.6. At inlet pressure of around 1319 kPa, the temperature difference at cold mass fraction of 0.61 is observed around 17.5°C. The temperature separation decreases once the cold mass fraction is beyond 0.8. The vortex tube produces higher temperature separation for the 4 CFM generator than the 2 CFM generator for similar inlet pressure.

8R generator

The experimental results obtained with R134a as working fluid for different inlet conditions using the 8R generator are shown in Figure 3.31, 3.32 and 3.33. Using the 8R generator enables the vortex tube to attain mass flow rate up to 13 g/s. However, at such operating condition, the vortex tube makes loud whistle even though it is fitted in a closed system. The temperature of both the cold and

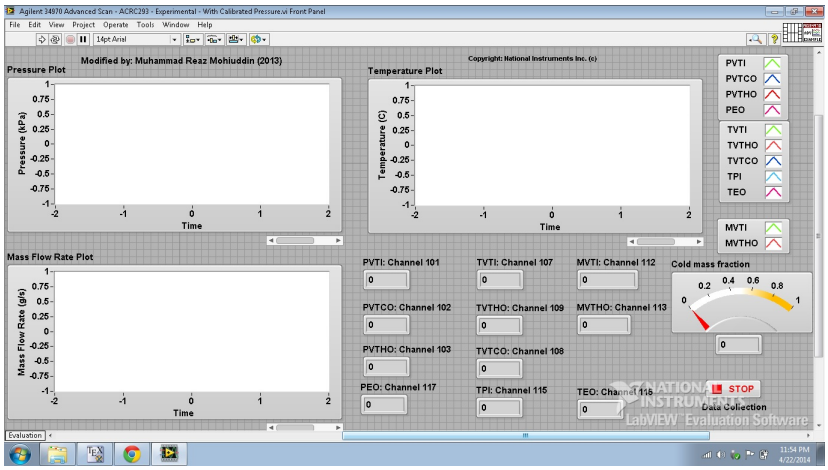

Figure 3.24: LABVIEW data acquisition software interface

the hot outlets increase with increase of cold mass fraction. However, the difference between the two outlet temperatures remain close to 10°C irrespective of operating condition. The vortex tube in this case acts as an isenthalpic expansion valve with closing and opening of the external valve that controls the cold mass fraction only makes subtle changes to the mass flow rate through the vortex tube only.

Performance analysis

From the pressure and temperature data collected at the inlet and the outlets of the vortex tube, thermodynamic properties are calculated. For comparing the expansion process in the vortex tube with an isenthalpic and an isentropic expansion device, actual cold outlet temperature is compared to the calculated isenthalpic and isentropic expansion temperature. Figure 3.34, 3.35 and 3.36 show that the vortex tube provides lower cold end temperature than an isenthalpic expansion device for 2R and 4R swirl generators. However, the cold end temperature is not as low as compared to an isentropic expansion device. For 2R generator, the temperature separation increases at higher cold mass fractions from 0.4 to 0.6. For 4R generator, similar trend is seen. However, beyond cold mass fraction of 0.8, there is not much difference between vortex tube cold side and calculated isenthalpic expansion temperature. For the 8R generator, although there are some temperature differences between the cold and the hot outlet, the cold outlet temperature is close to isenthalpic expansion temperature which indicates that, the vortex tube

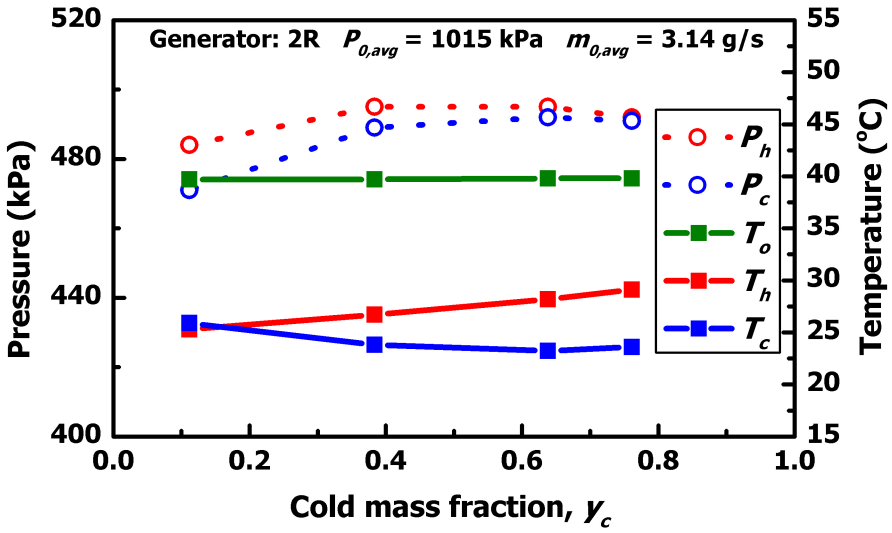

Figure 3.25: Temperature variation at vortex tube inlet and two outlets using 2R generator for mean inlet pressure of 1015 kPa (standard deviation = 1.5 kPa). The mean mass flow is 3.14 g/s (standard deviation = 0.034 g/s)

acts as an expansion valve while 8R generator is used. This phenomenon can be attributed to existence of more saturated liquid droplets at the vortex tube inlet than the other two generators.

For the 2R and 4R generators, temperature at the cold end is lower than the isenthalpic expansion temperature by 4 to 8°C. However, for 8R generator, the temperature drop is closer to that of an isenthalpic expansion device.

Eiamsa-ard and Promvonge [12] used the principle of adiabatic expansion of ideal gas to calculate the cold side efficiency of vortex tube where expansion is assumed to occur in isentropic process in ideal case. Isentropic efficiency involves the comparison between the actual performance of a device and the performance that would be achieved under idealized circumstances for the same inlet and outlet state. However, the refrigerant R134a not being a fluid behaving like ideal gas in its own gaseous state makes it difficult to calculate the isentropic efficiency using Equation 2.2. The isentropic efficiency is calculated in this case by using Equation 3.3.

$$\eta_{c,isen} = \frac{h_o - h_c}{h_o - h_{c,isen}} \tag{3.3}$$

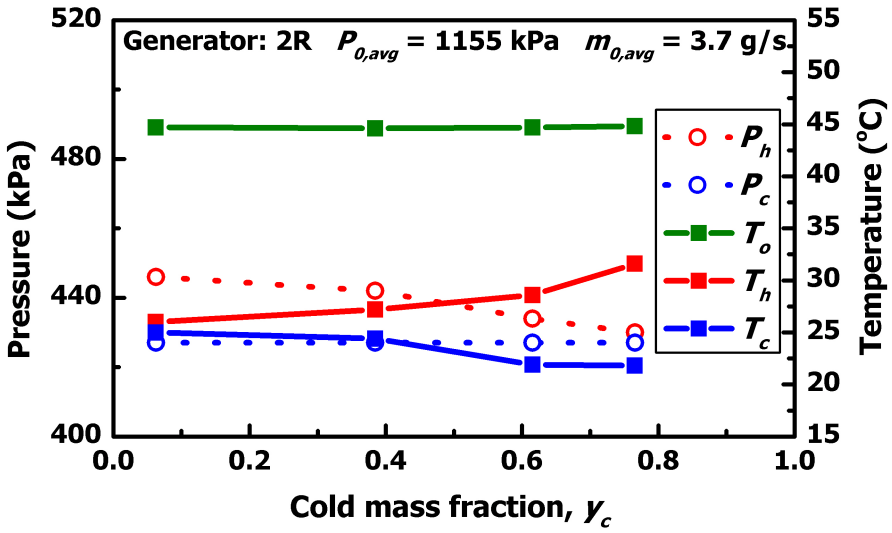

Figure 3.26: Temperature variation at vortex tube inlet and two outlets using 2R generator for mean inlet pressure of 1155 kPa (standard deviation = 4 kPa). The mean mass flow is 3.7 g/s (standard deviation = 0.33 g/s)

The isentropic efficiencies are shown in Figures 3.37, 3.38 and 3.39 for the three sizes of vortex generators. The results are shown at different average inlet pressure to show the variation of isentropic efficiency with inlet pressure. The maximum efficiency observed is around 33% observed during experimentation with the 2R and 4R generator. The maximum efficiency observed while using an 8R generator around 12%. For the 4R generator, the efficiency peaks at a range of cold mass fraction between 0.4 and 0.6. Similar trend is also observed with experiments with air.

The cooling capacity of the vortex tube for the three swirl generators while using R134a is calculated using Equation 3.1. The results are shown in Figure 3.40, 3.41 and 3.42. The results indicate an increasing trend of cooling capacity with cold mass fraction. Increment of cold mass fraction increases the amount of mass flow through the cold outlet and also for the refrigerant, the temperature separation does not vary by a significant amount. Therefore, the effect of increased mass flow has more influence on the result than the difference of specific enthalpy between the inlet and the cold outlet.

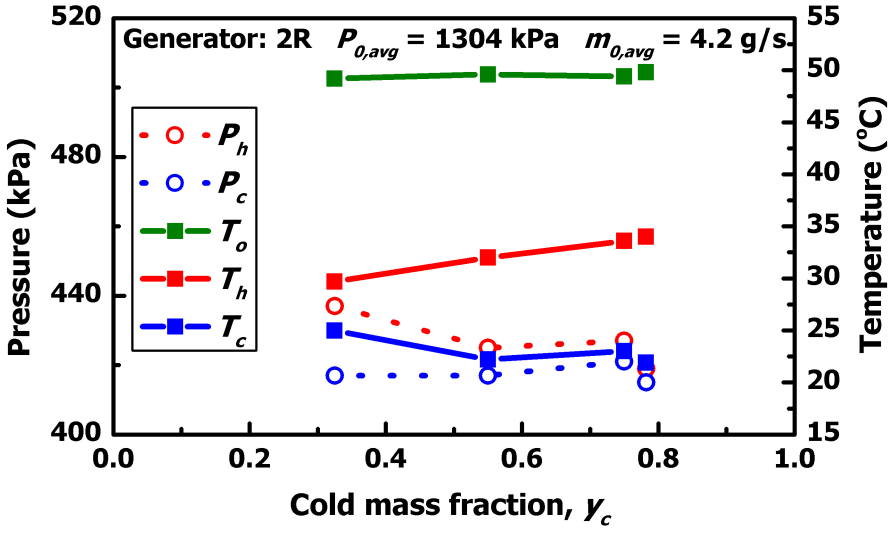

Figure 3.27: Temperature variation at vortex tube inlet and two outlets using 2R generator for mean inlet pressure of 1304 kPa (standard deviation = 2.38 kPa). The mean mass flow is 4.2 g/s (standard deviation = 0.26 g/s)

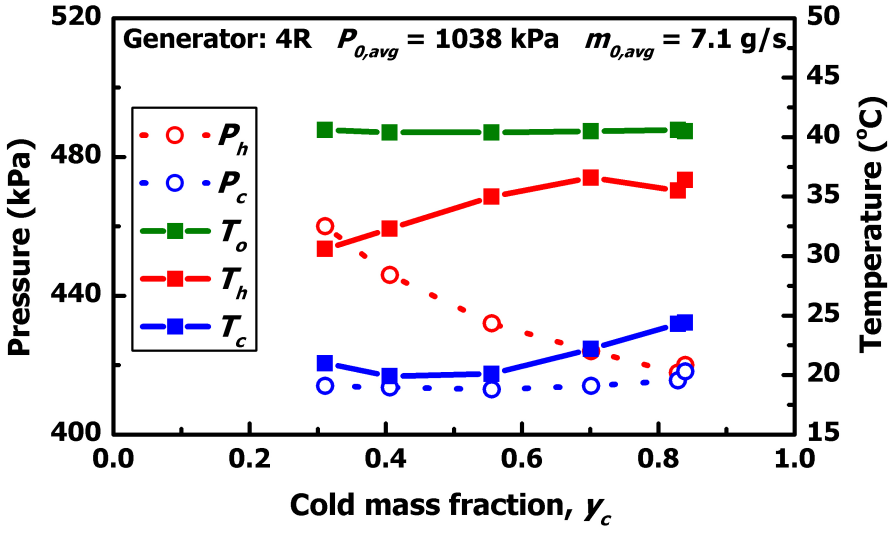

Figure 3.28: Temperature variation at vortex tube inlet and two outlets using 4R generator for mean inlet pressure of 1038 kPa (standard deviation = 1.71 kPa). The mean mass flow is 7.1 g/s (standard deviation = 0.7 g/s)

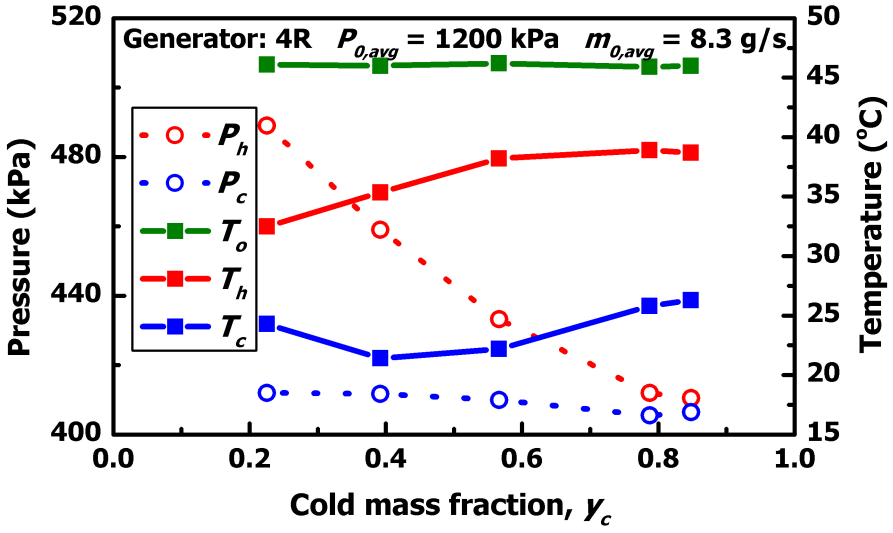

Figure 3.29: Temperature variation at vortex tube inlet and two outlets using 4R generator for mean inlet pressure of 1200 kPa (standard deviation = 2.16 kPa). The mean mass flow is 8.3 g/s (standard deviation = 0.28 g/s)

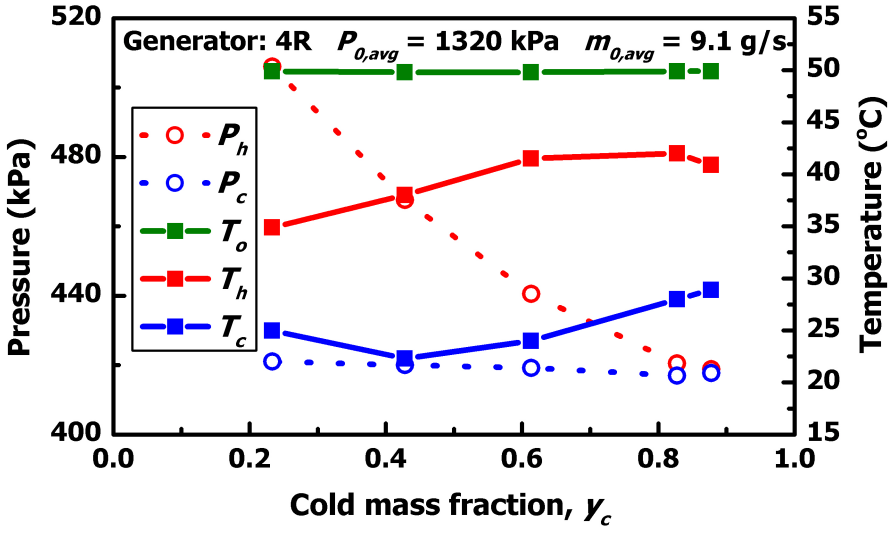

Figure 3.30: Temperature variation at vortex tube inlet and two outlets using 4R generator for mean inlet pressure of 1321 kPa (standard deviation = 2.1 kPa). The mean mass flow is 9.1 g/s (standard deviation = 0.29 g/s)

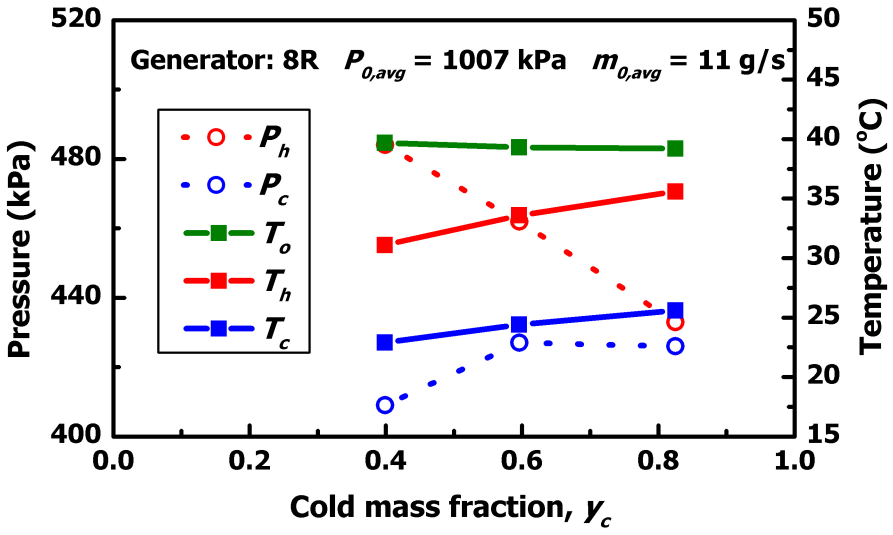

Figure 3.31: Temperature variation at vortex tube inlet and two outlets using 8R generator for mean inlet pressure of 1007 kPa (standard deviation = 7 kPa). The mean mass flow is 11 g/s (standard deviation = 0.12 g/s)

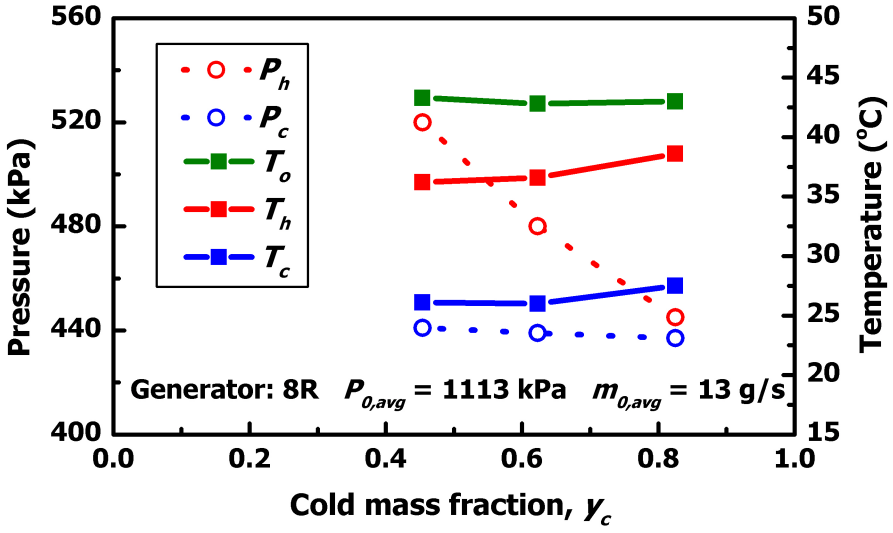

Figure 3.32: Temperature variation at vortex tube inlet and two outlets using 8R generator for mean inlet pressure of 1113 kPa (standard deviation = 4 kPa). The mean mass flow is 13 g/s (standard deviation = 0.58 g/s)

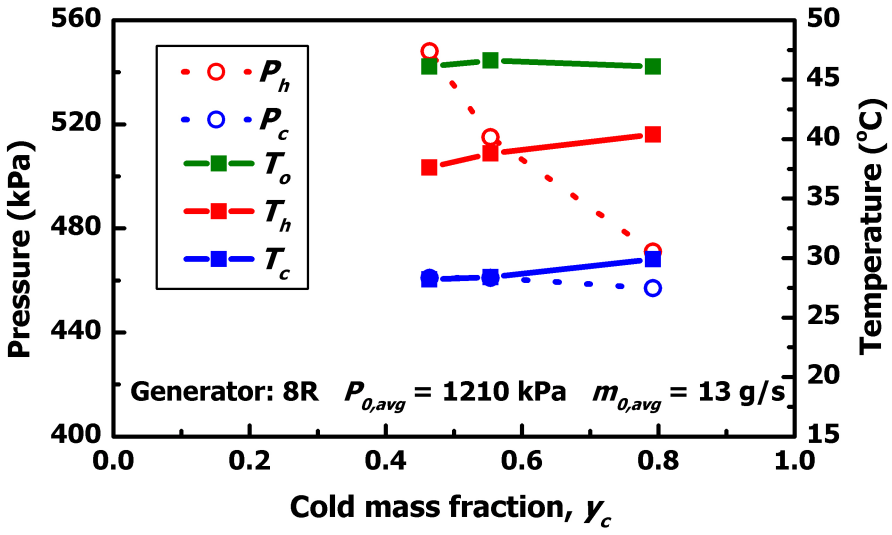

Figure 3.33: Temperature variation at vortex tube inlet and two outlets using 8R generator for mean inlet pressure of 1210 kPa (standard deviation = 4.7 kPa). The mean mass flow is 13 g/s (standard deviation = 0.58 g/s)

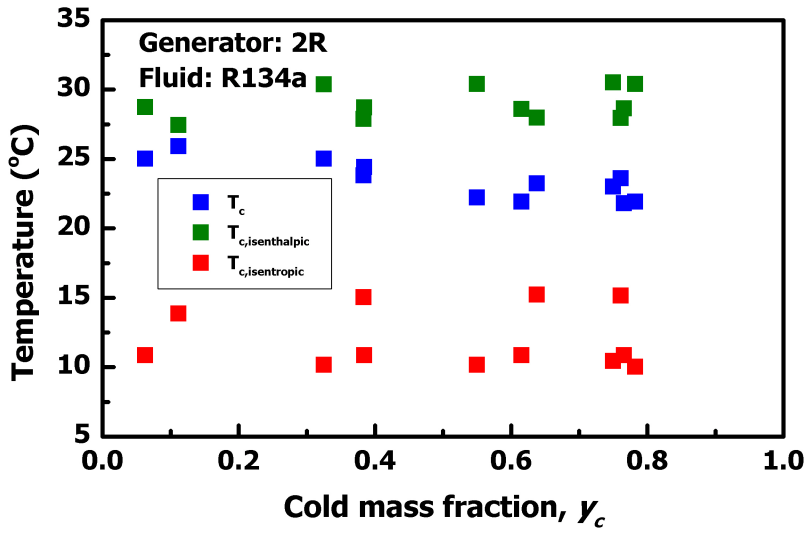

Figure 3.34: Comparison of actual vortex tube cold end temperature with isenthalpic and isentropic expansion between operated between the inlet and outlet pressures using an 2R generator and R134a

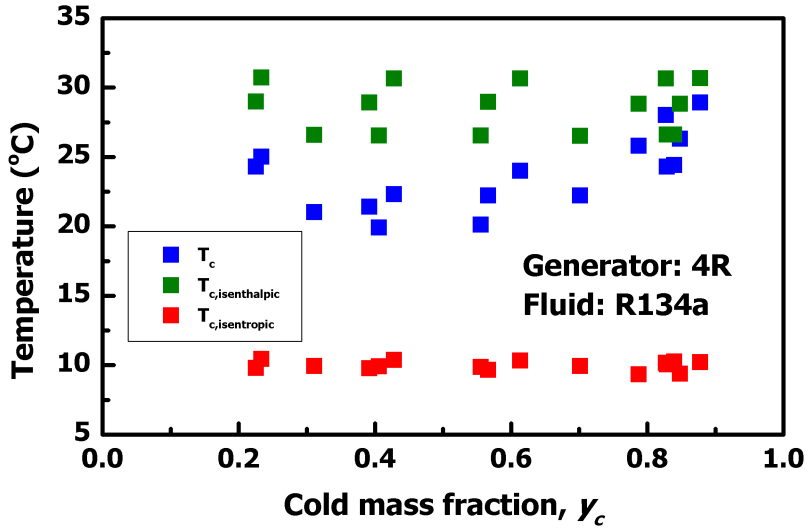

Figure 3.35: Comparison of actual vortex tube cold end temperature with isenthalpic and isentropic expansion between operated between the inlet and outlet pressures using an 4R generator and R134a

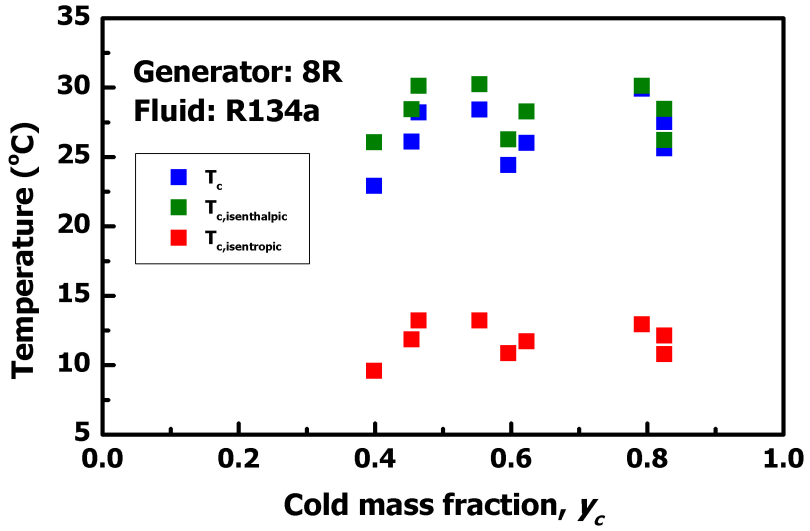

Figure 3.36: Comparison of actual vortex tube cold end temperature with isenthalpic and isentropic expansion between operated between the inlet and outlet pressures using an 8R generator and R134a

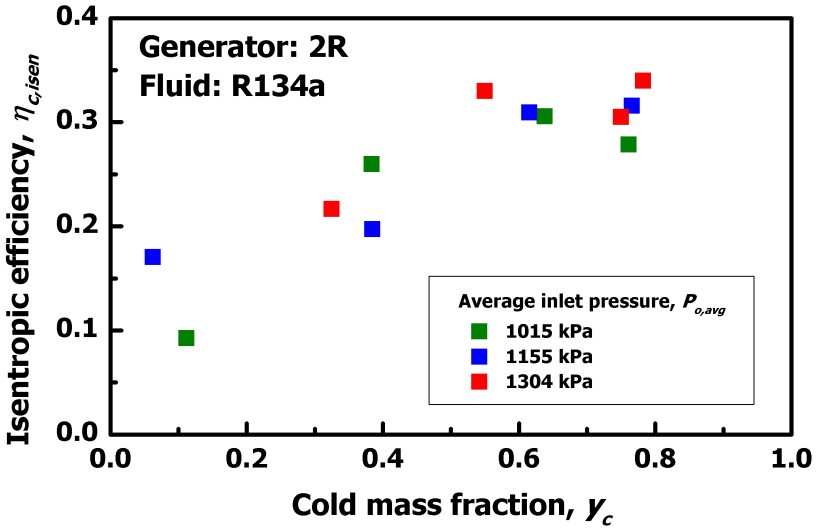

Figure 3.37: Isentropic efficiency of vortex tube using an 2R generator and R134a as working fluid

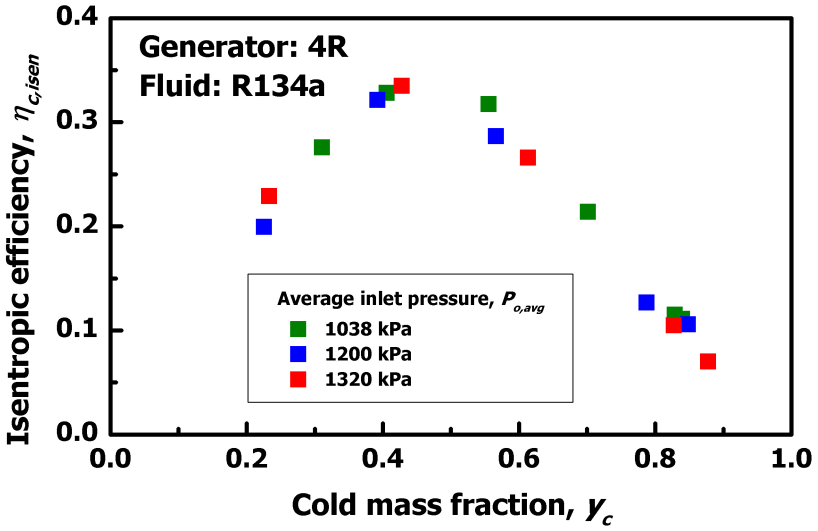

Figure 3.38: Isentropic efficiency of vortex tube using an 4R generator and R134a as working fluid

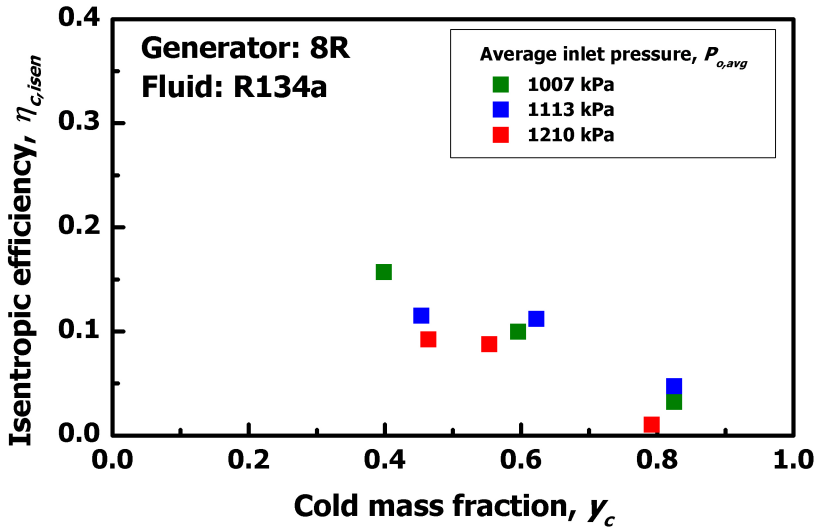

Figure 3.39: Isentropic efficiency of vortex tube using an 8R generator and R134a as working fluid

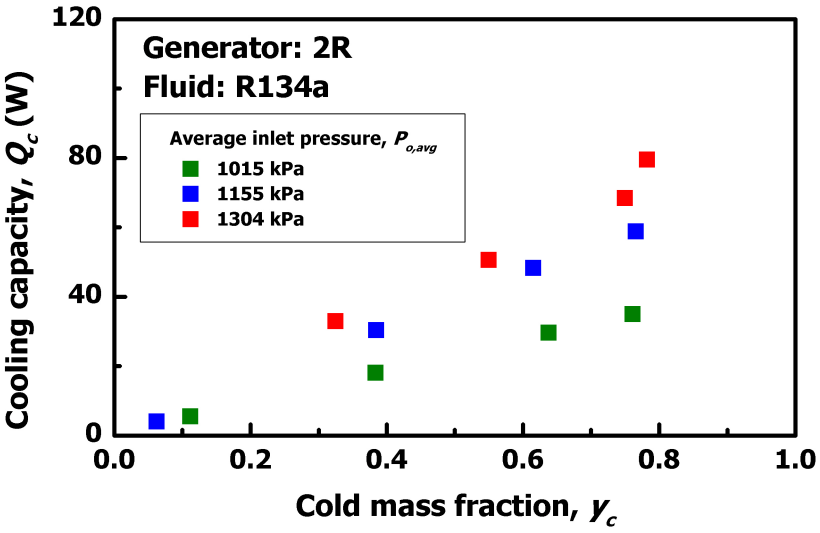

Figure 3.40: Cooling capacity of the cold outlet using an 2R generator and R134a

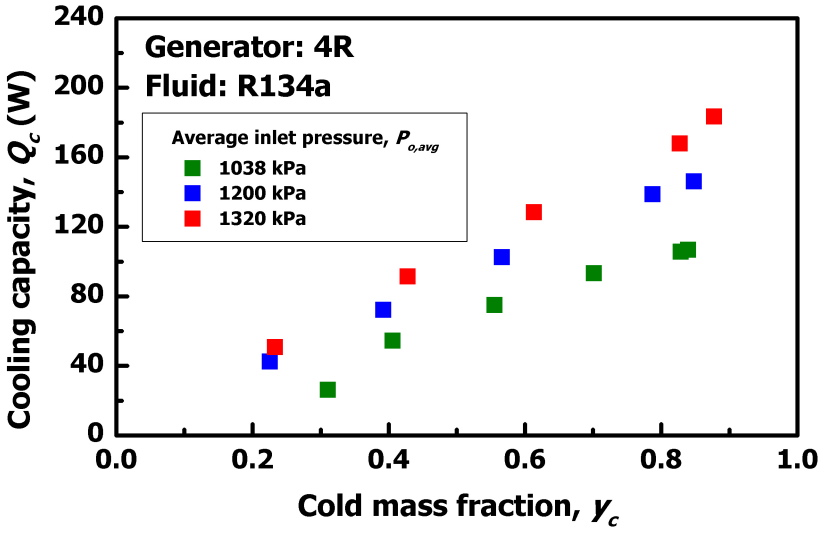

Figure 3.41: Cooling capacity of the cold outlet using an 4R generator and R134a

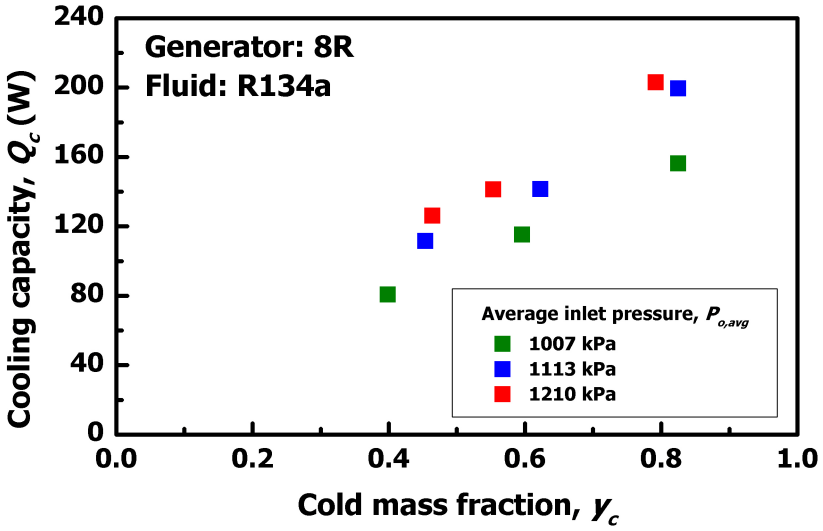

Figure 3.42: Cooling capacity of the cold outlet using an 8R generator and R134a

CHAPTER 4

NUMERICAL INVESTIGATION OF NOVEL VORTEX TUBE CYCLE

This chapter describes the numerical work carried out to simulate the performance of a proposed refrigeration cycle utilizing the vortex tube to achieve more subcooling. The calculation routine is described in detail. The vortex tube is implemented into the thermodynamic cycle analysis. The potential of the novel cycle in improving the COP is investigated through the system model.

4.1 Proposed vortex tube subcooling cycle

From the literature review, it is understood that the vortex tube demonstrates temperature separation between the two outlets when operated with inlet at high pressure and flowing fluid being mostly vapor. Also, from the experimental work conducted, it is evident that with R134a, there is temperature separation of the hot and cold outlet when operated at high inlet pressure. Therefore, while operating with the refrigerant in a vapor compression cycle, the vortex tube will be better suited if utilized on the high pressure side. In the proposed vortex tube cycle as shown in Figure , the vortex tube is used along with a separator after the condenser. The portion of refrigerant that has not condensed inside the condenser is separated using the separator. The refrigerant vapor is supplied to the inlet of the vortex tube. The refrigerant that is entering the vortex tube is at high pressure and in saturated vapor state. The refrigerant expands in the vortex tube and is separated in to a cold stream and another stream that is hotter than the cold stream. The cold and the hot outlets of the vortex tube are supplied to two different subcoolers that are both heat exchangers. The saturated liquid refrigerant extracted by the separator is also flown through the subcoolers. This enables the increased subcooling of the liquid refrigerant before entering the expansion device. The increased subcooling also increases the cooling capacity of the evaporator without raising the high side pressure which is normally done to achieve more subcooling. Refrigerant passing

through the vortex tube cold outlet and evaporator are mixed again before the compressor inlet. The hot outlet of the vortex tube is passed through another heat exchanger before mixing it with the vortex tube cold outlet and evaporator outlet refrigerant. The mixture is then passed into the compressor and then to the condenser. This cycle also prevents the saturated vapor from the condenser from accessing the evaporator affect refrigerant distribution.

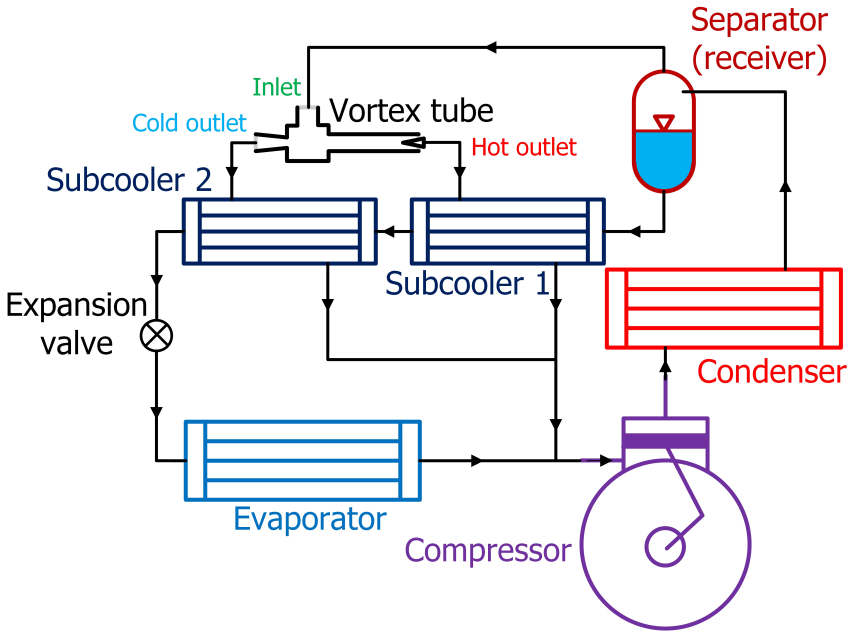

Figure 4.1: Increased subcooling in vapor compression refrigeration cycle using vortex tube

4.2 Thermodynamic cycle analysis

A thermodynamic cycle analysis is carried out to assess the COP improvement potentials for refrigeration system using the proposed vapor compression cycle with vortex tube subcooling. EES (2013) software is used in simulating the performance of the cycle. The results are then compared to a regular vapor compression cycle. The software package used provides two major advantages. Firstly, the integrated Newton-Raphson solver allows for implicit programming of model equations. Secondly, simple function calls can be used to conveniently incorporate thermodynamic properties of a large number of substances. In the case of R134a, the high-accuracy Tilner-Roth and Baehr [13] equation of state is used to

directly link the desired refrigerant properties to the model equation.

The calculations are carried out for R134a to investigate the COP improvement potentials due to expansion work recovery. The thermodynamic cycle analysis is based on the following assumptions:

- Isentropic efficiency of the compressor is assumed to be 0.8
- Condensation at saturation pressure corresponding to ambient temperature. At the outlet of the condenser, some portion of the refrigerant remains in the saturated vapor phase
- For calculating the fluid outlet temperature in the subcoolers by assuming the heat exchanger effectiveness, η is assumed to be 0.8
- Isenthalpic expansion in the expansion device used in both proposed and the baseline cycle
- Isobaric heat absorption in the evaporator; evaporation at saturation pressure corresponding to the surrounding ambient temperature. A superheat of 5°C is assumed in the evaporator exit
- Heat conduction and viscosity effects are neglected
- Gravitational potential energy is neglected while using the energy balance

In the thermodynamic model, the temperature in the evaporator and the condenser are set in the beginning which sets up the high side and the low side pressure. The cooling capacity of the evaporator is fixed at 4 kW. The setting of cooling capacity determines the mass flow rates. The outlet quality of the condenser refrigerant is set to 0.2. The refrigerant at the inlet of the vortex tube is saturated vapor with the same temperature and pressure as in the condenser. The cold mass fraction is also provided taking into consideration, the most suitable operating points from the experiments which is 0.6. The isentropic efficiency of the cold side is assumed to be 0.35 which is obtained from the experimental investigation. The mass flow rates of the hot and the cold sides are calculated using Equation 4.1 and the mass balance in Equation 4.2

$$\dot{m}_c = y_c \cdot \dot{m}_o \tag{4.1}$$

$$\dot{m}_o = \dot{m}_c + \dot{m}_h \tag{4.2}$$

Using the isentropic efficiency from the experimental investigation, the cold side specific enthalpy is calculated using Equation 3.3. The specific enthalpy of the cold side for isentropic expansion is calculated using EES (2013) by taking into consideration the specific entropy of the inlet and then calculating the specific enthalpy at cold outlet using the outlet pressure and inlet specific entropy.

The vortex tube hot outlet enthalpy is calculated using an energy balance using Equation 4.3. The outlet pressures for both sides are set to the evaporator pressure. Using the enthalpy and the pressure values at the outlets, other properties are determined using the EES (2013) database.

$$\dot{m}_o \cdot h_o = \dot{m}_c \cdot h_c + \dot{m}_h \cdot h_h \tag{4.3}$$

In the both the subcoolers, outlet temperatures of both the fluids are calculated by assuming the heat exchanger effectiveness, and conducting heat balance. The cooling capacity of the evaporator is used to determine the mass flow rate through it. Properties of the inlet fluid to the compressor is determined by using the energy balance at the mixing point of evaporator and subcooler outlets. Finally, the COP of the system is determined using Equation 4.4

$$COP = \frac{\dot{Q}_{er}}{\dot{W}_{cp}} \tag{4.4}$$

The simulation is run for the baseline and vortex tube subcooling cycle with varying the condenser outlet quality. For the simulation, the cold mass fraction is kept fixed at 0.6. Also, the isentropic efficiency of the vortex tube cold outlet is set to 0.35 as found in the experimental study. The evaporator temperature is fixed at 10°C and condenser temperature is fixed at 50°C. The corresponding saturation pressure for the evaporator and condenser temperatures are 415 kPa and 1319 kPa respectively. The result of the simulation is shown in Figure 4.2. The results indicate that COP decreases as the condenser outlet quality increases. On the other hand, the total refrigerant mass flow rate increases with increasing condenser outlet quality. For the vortex tube subcooling cycle the decrease in COP and increase in total refrigerant mass flow rate both are lower compared to

the baseline cycle.

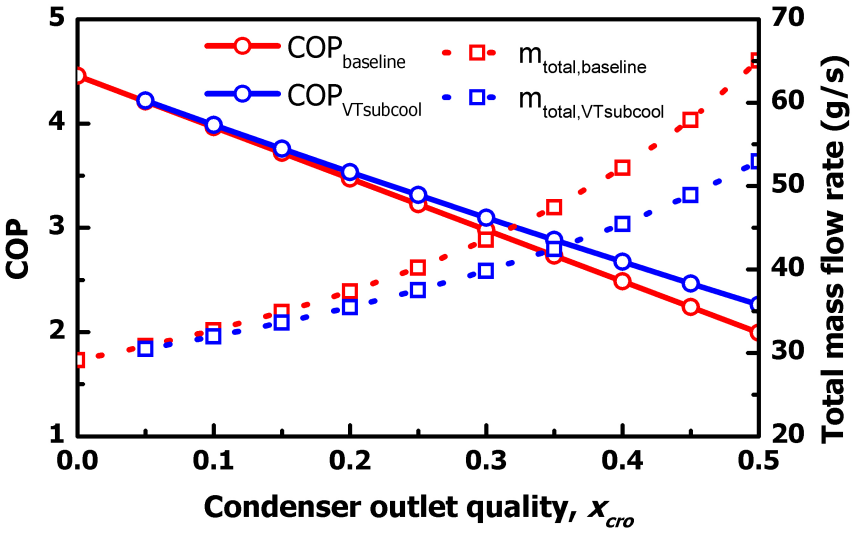

Figure 4.2: Variation of COP and total refrigerant mass flow rate with increasing condenser outlet quality

For variation of the condenser temperature, the results shown in Figure 4.3 show that in both cases, the COP of the two cycles decrease in a similar way, with vortex tube subcooling cycle in a slight advantage. However, the subcooling cycle requires less refrigerant mass flow than the baseline cycle. For this simulation, the condenser outlet quality is set to 0.1. Evaporator temperature is set at 10°C. The vortex tube cold outlet isentropic efficiency and the cold mass fraction have been set to 0.35 and 0.6 respectively.

The variation of COP and total refrigerant mass flow rate at different evaporator temperature is shown in Figure 4.4. The condenser temperature is kept fixed at 50°C. The vortex tube parameters remain the same as for the simulation with varying condenser temperature shown in Figure 4.3. The results show that, COP of both the baseline and the vortex tube subcooling cycle increase similarly with the increase of evaporator temperature. The vortex tube cycle requires lower refrigerant mass flow rate than the baseline cycle.

Variation of COP and total refrigerant mass flow rate with different vortex tube cold mass fractions were simulated and compared with the baseline cycle performance at similar conditions. The evaporator and condenser temperatures have been fixed at 10°C and 50°C respectively. Condenser outlet quality is set to 0.1.

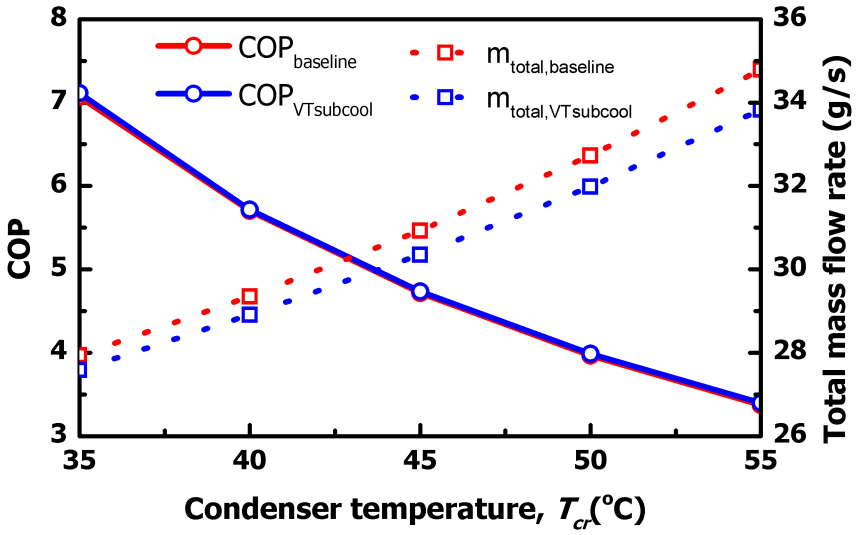

Figure 4.3: Variation of COP and total mass flow rate with varying condenser temperature

The cooling capacity of the evaporator is set to 4 kW. The vortex tube cold side efficiency is 0.35. The results are shown in Figure which indicate that the COP and total refrigerant mass flow rates are do not alter to any significant level if the cold mass fraction is varied. However, the mass flow rate required for the desired cooling capacity is lower in case of the vortex tube subcooling cycle than that of the baseline cycle.

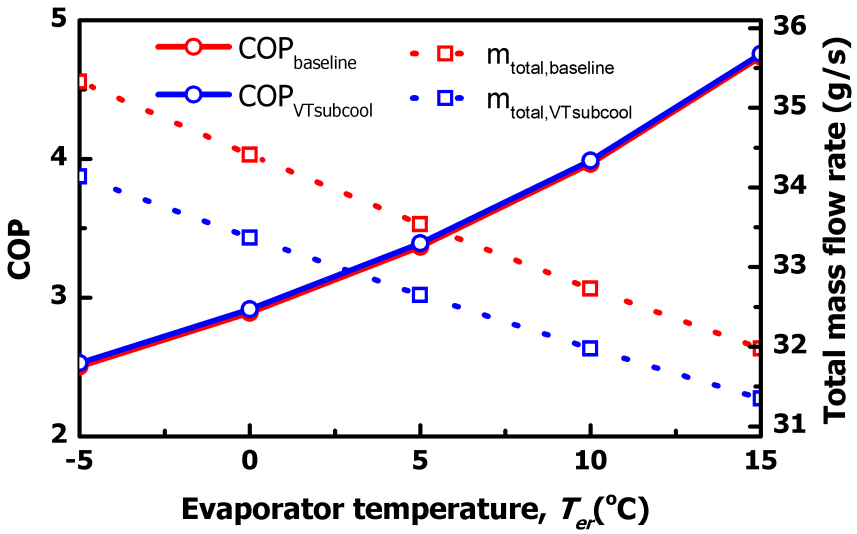

Figure 4.4: Variation of COP and total refrigerant mass flow rate with evaporator temperature

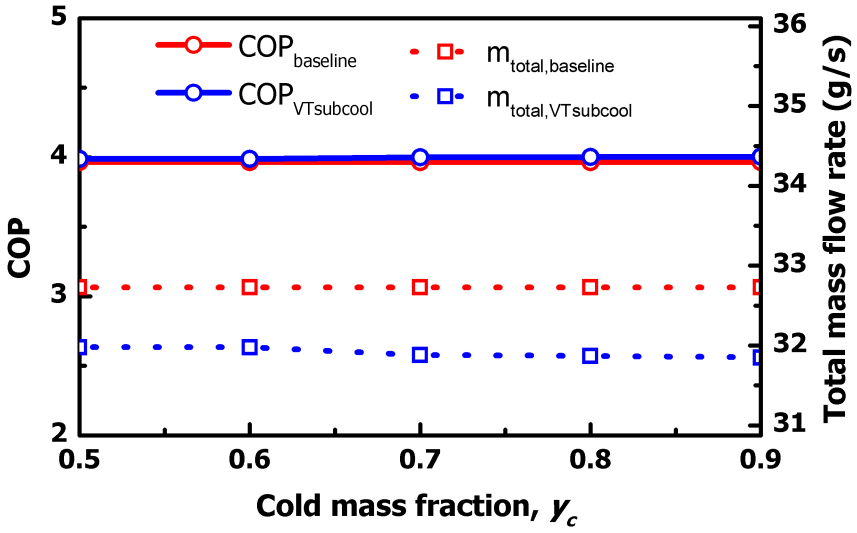

Figure 4.5: Variation of COP and total refrigerant mass flow rate of the vortex tube subcooling cycle with baseline cycle

CHAPTER 5

CONCLUSIONS AND FUTURE WORK

The thesis has described a study to investigate the vortex tube application for refrigerant in order to improve performance of the refrigeration system. A commercially available vortex tube is tested with different working fluids i.e. air and refrigerant R134a to get a thorough understanding of possible operating conditions. Based upon the experimental investigation results, a new refrigeration cycle has been proposed. A numerical model is developed to estimate the performance improvement due to incorporation of vortex tube in to the new cycle.

The experimental investigation shows that the vortex tube can achieve temperature differences for air and R134a. The cold side temperature is found to be lower than the isenthalpic expansion temperature which shows the potential to recover work. In case of the refrigerant, the hot end outlet temperature of the working fluid does not climb above that of the inlet temperature. Although the hot side temperature does not climb above the inlet temperature, the reason might be operating conditions being close to saturation. Also, temperature separation is higher at higher inlet pressure and higher inlet quality. However, the maximum hot and minimum cold outlet temperatures cannot be achieved at the same hot end valve setting. Also, the maximum isentropic efficiency for the cold outlet is achieved at completely different hot end valve setting. The vortex tube has different sizes of swirl generators for achieving different mass flow rates. The performance of the vortex tube is affected by the size of the swirl generator. For the vortex tube used in the study, the 4R generator provided the highest temperature separation for R134a. The isentropic efficiency of the vortex tube operating with R134a for 4R generator is observed to reach up to 34% with a temperature difference between cold and hot outlet of 17°C.

From the numerical simulation of the vortex tube subcooling cycle and comparing it to the baseline cycle, it is evident that the most influential parameter is

the condenser outlet quality provided the efficiency of the vortex tube cold outlet remains consistent at those operating conditions. Even though higher condenser outlet quality of refrigerant helps the subcooling cycle to achieve better COP than the baseline cycle, the magnitude of COP values decrease as a result of split in the condenser outlet mass. The vortex tube subcooling cycle requires less mass flow rate requirement than the baseline system.

There is still much potential for future research concerning application of vortex tube in refrigeration. The thesis has described a novel cycle that can operate with the current commercially available vortex tube with refrigerant and yield better performance than the conventional vapor compression cycle. Modification of the experimental setup will enable to take accurate measurement of the inlet refrigerant vapor quality and even operate at superheated inlet condition that will further enable further insight into the work recovery capabilities of the vortex tube. The very promising results obtained in this study warrant further investigation on the cycle level. For that purpose, the novel cooling cycles has been proposed, with the aim of implementing single-phase vortex tube operation in realistic HVAC&R applications.

APPENDIX A

EXPERIMENTAL DATA

This appendix presents the raw experimental data for vortex tube performance tests using air and refrigerant R134a. The data points presented in Table A.1 up to Table A.9 represent vortex tube hot and cold outlet temperature data collected while using air as working fluid for three different swirl generators at different inlet pressures. Both the outlet pressures for experiments with air is atmospheric. Table A.10 contains mass flow rate data at different inlet pressure through the vortex tube at hot outlet fully open condition. The performance data for R134a using 2R, 4R and 8R generators are provided in Tables A.11, A.12 and A.13 respectively.

Table A.1: Vortex tube performance data with 2R swirl generator using air as working fluid at inlet pressure close to 400 kPa

y_c	P_o (kPa)	T_h (°C)	T_c (°C)
0.04	390	26	13
0.18	414	29	8
0.23	394	32	7
0.46	397	39	6
0.57	395	40	7
0.69	392	40	9
0.87	394	35	13
0.94	405	32	15
1.00	410	22	17
1.00	408	24	19

Table A.2: Vortex tube performance data with 2R swirl generator using air as working fluid at inlet pressure close to 600 kPa

y_c	P_o (kPa)	T_h (°C)	T_c (°C)
0.03	607	22	22
0.11	598	23	14
0.16	590	25	10
0.25	601	30	2
0.31	604	36	-3
0.33	604	35	-2
0.42	607	43	-4
0.50	602	46	-3
0.58	603	51	-2
0.65	603	53	1
0.75	600	53	4
0.79	603	51	7
0.93	604	42	13
1.00	605	23	18
1.00	605	24	18

Table A.3: Vortex tube performance data with 2R swirl generator using air as working fluid at inlet pressure close to 800 kPa

y_c	P_o (kPa)	T_h (°C)	T_c (°C)
0.01	815	22	22
0.06	824	24	14
0.13	815	30	2
0.21	815	36	-5
0.26	825	40	-8
0.61	820	66	-4
0.66	820	68	-1
0.75	819	69	3
0.80	822	68	6
0.86	822	62	10
0.92	817	55	13
0.97	765	22	18
0.97	814	24	18

Table A.4: Vortex tube performance data with 4R swirl generator using air as working fluid at inlet pressure close to 400 kPa

y_c	P_o (kPa)	T_h (°C)	T_c (°C)
0.01	411	24	14
0.14	411	29	8
0.18	411	31	5
0.29	413	36	2
0.37	429	40	0
0.41	401	42	1
0.54	414	47	3
0.55	400	42	1
0.60	410	50	6
0.60	403	49	4
0.68	418	51	7
0.74	402	51	10
0.85	411	48	13
0.89	407	42	16
0.96	388	29	21
0.97	400	27	20

Table A.5: Vortex tube performance data with 4R swirl generator using air as working fluid at inlet pressure close to 600 kPa

y_c	P_o (kPa)	T_h (°C)	T_c (°C)
0.05	615	22	13
0.12	615	25	8
0.13	613	22	22
0.18	594	28	1
0.29	619	35	-6
0.35	617	41	-7
0.41	613	44	-7
0.48	598	49	-6
0.52	616	52	-4
0.60	618	56	-2
0.64	612	56	-4
0.68	611	59	0
0.70	615	62	-1
0.79	608	65	7
0.87	615	60	10
0.96	610	45	15
0.98	606	34	18
0.98	595	32	20

Table A.6: Vortex tube performance data with 4R swirl generator using air as working fluid at inlet pressure close to 780 kPa

y_c	P_o (kPa)	T_h (°C)	T_c (°C)
0.08	736	23	11
0.16	800	24	11
0.20	741	32	-7
0.38	781	45	-10
0.48	794	53	-10
0.53	792	60	-8
0.60	791	64	-5
0.65	804	67	-6
0.69	792	69	-2
0.71	751	71	-1
0.76	792	71	3
0.87	792	67	10
0.96	790	38	17
0.98	804	42	20

Table A.7: Vortex tube performance data with 8R swirl generator using air as working fluid at inlet pressure close to 400 kPa

y_c	P_o (kPa)	T_h (°C)	T_c (°C)
0.00	407	22	22
0.21	406	25	10
0.74	407	63	4
0.81	408	67	7
0.98	407	32	21

Table A.8: Vortex tube performance data with 8R swirl generator using air as working fluid at inlet pressure close to 600 kPa

y_c	P_o (kPa)	T_h (°C)	T_c (°C)
0.09	596	22	29
0.31	603	36	-6
0.77	608	83	2
0.84	618	89	6
0.99	604	39	21

Table A.9: Vortex tube performance data with 8R swirl generator using air as working fluid at inlet pressure close to 700 kPa

y_c	P_o (kPa)	T_h (°C)	T_c (°C)
0.14	700	24	17
0.34	662	39	-8
0.77	695	86	1
0.84	708	92	5
0.99	684	44	20
0.99	721	45	20

Table A.10: Vortex tube mass flow rate data with 2R, 4R and 8R swirl generator using air as working fluid at different inlet pressure with hot end fully open. The average inlet air temperature is 23.3°

2R	2R	4R	4R	8R	8R
P_o (kPa)	m_o (g/s)	P_o (kPa)	m_o (g/s)	P_o (kPa)	m_o (g/s)
192	0.5327	196	1.015	197	1.864
197	0.5465	197	1.02	198	2.155
202	0.5604	201	1.041	203	2.211
215	0.692	205	1.008	204	1.943
294	1.518	206	1.067	211	2.293
298	1.447	298	3.101	304	5.431
304	1.721	300	3.108	305	5.508
311	1.761	310	2.945	306	6.404
312	1.766	311	3.207	309	6.047
395	3.049	317	3.314	313	6.202
405	3.261	398	6.077	406	11.470
408	3.104	400	5.911	407	11.720
410	3.301	400	5.613	407	10.990
414	3.448	403	5.783	407	10.600
425	3.634	413	6.673	408	10.970
508	5.926	493	9.419	496	17.260
510	5.552	498	9.041	507	18.700
511	5.847	508	9.211	511	18.170
521	6.077	509	9.53	511	17.890
527	6.499	519	10.53	532	19.820
599	8.187	595	13.47	596	24.460
600	8.468	609	15.31	603	25.050
603	8.711	612	15.25	604	23.710
606	8.653	613	15.99	608	24.850
606	8.047	615	14.51	618	25.460
607	8.668	700	18.1	662	30.130
693	10.78	704	19.37	684	30.510
693	10.59	707	18.17	695	32.340
704	11.88	708	18.96	700	33.860
711	11.46	709	19.61	708	33.780
717	12.35	751	21.35	721	34.330
767	11.68	753	22.54		
808	14.38	800	25.61		
809	14.35	804	25.02		
811	14.52	804	23.24		
815	14.59				
818	14.33				

Table A.11: Vortex tube performance data with 2R swirl generator using R134a as working fluid

P_o kPa	P_h kPa	P_c kPa	T_o °C	T_h °C	T_c °C	T_{rpi} °C	$\dot{m}_o$ g/s	$\dot{m}_h$ g/s	y_c	N_{rp} Hz
1159	446	427	45	26	25	8	3.20	3.00	0.06	17.00
1157	442	427	45	27	24	8	3.90	2.40	0.38	17.00
1150	434	427	45	29	22	8	3.90	1.50	0.62	17.00
1154	430	427	45	32	22	8	3.80	0.89	0.77	17.00
1301	437	417	49	30	25	7	4.00	2.70	0.33	15.50
1302	425	417	50	32	22	7	4.00	1.80	0.55	16.00
1305	427	421	49	34	23	7	4.40	1.10	0.75	16.00
1306	419	415	50	34	22	7	4.50	0.98	0.78	16.00

Table A.12: Vortex tube performance data with 4R swirl generator using R134a as working fluid

P_o kPa	P_h kPa	P_c kPa	T_o °C	T_h °C	T_c °C	T_{rpi} °C	$\dot{m}_o$ g/s	$\dot{m}_h$ g/s	y_c	N_{rp} Hz
1040	460	414	41	31	21	7	7.27	5.01	0.31	18.00
1037	446	414	40	32	20	7	7.17	4.26	0.41	18.00
1038	432	413	40	35	20	7	7.20	3.20	0.56	18.00
1036	424	414	41	37	22	7	7.10	2.12	0.70	18.00
1040	418	416	41	36	24	7	6.84	1.17	0.83	18.00
1036	420	418	41	36	24	7	6.86	1.10	0.84	18.00
1201	489	412	46	33	24	7	8.65	6.70	0.23	18.00
1198	459	412	46	35	21	7	8.52	5.18	0.39	18.00
1203	433	410	46	38	22	7	8.30	3.60	0.57	18.00
1200	412	406	46	39	26	7	8.00	1.70	0.79	18.00
1198	411	406	46	39	26	7	7.90	1.20	0.85	18.00
1321	506	421	50	35	25	7	9.39	7.20	0.23	18.00
1318	468	420	50	38	22	7	9.23	5.28	0.43	18.00
1319	441	419	50	42	24	7	9.05	3.50	0.61	18.00
1323	421	417	50	42	28	7	8.70	1.50	0.83	18.00
1324	419	418	50	41	29	7	9.00	1.10	0.88	18.00

Table A.13: Vortex tube performance data with 8R swirl generator using R134a as working fluid

P_o kPa	P_h kPa	P_c kPa	T_o °C	T_h °C	T_c °C	T_{rpi} °C	$\dot{m}_o$ g/s	$\dot{m}_h$ g/s	y_c	N_{rp} Hz
1015	484	409	40	31	23	6	10.98	6.60	0.40	18.00
1004	462	427	39	34	24	6	11.11	4.49	0.60	18.00
1002	433	426	39	36	26	6	10.88	1.90	0.83	18.00
1110	480	439	43	37	26	6	13.00	4.90	0.62	18.00
1113	445	437	43	39	28	6	12.00	2.10	0.83	18.00
1118	441	522	43	36	26	6	13.00	7.10	0.45	18.00
1205	548	461	46	38	28	6	14.00	7.50	0.46	18.00
1214	515	461	47	39	28	6	13.00	5.80	0.55	18.00
1212	471	457	46	40	30	6	13.00	2.70	0.79	18.00
1239	576	471	47	41	32	6	14.00	8.30	0.41	18.00
1266	519	472	48	43	32	6	14.00	5.40	0.61	18.00
1278	484	473	48	46	34	6	14.00	2.40	0.83	18.00

REFERENCES

[1] R. Hilsch, "The use of the expansion of gases in a centrifugal field as cooling process," *Review of Scientific Instruments*, vol. 18, pp. 108–113, 1947.

[2] D. Robinson and E. Groll, "Efficiencies of transcritical CO_2 cycles with and without an expansion turbine," *International Journal of Refrigeration*, vol. 21, no. 7, pp. 577–589, 1998.

[3] N. Lawrence and S. Elbel, "Experimental and analytical investigation of automotive ejector air-conditioning cycles using low-pressure refrigerants," in *Proceedings of the International Refrigeration and Air Conditioning Conference*, no. 1169, Purdue University. West Lafayette, IN: Purdue e-Pubs, July 2012.

[4] K. Stephan, S. Lin, M. Durst, F. Huang, and D. Seher, "An investigation of energy separation in a vortex tube," *International Journal of Heat and Mass Transfer*, vol. 26, no. 3, pp. 341 – 348, 1983.

[5] O. Aydin, B. Markal, and M. Avci, "A new vortex generator geometry for a counter-flow Ranque-Hilsch vortex tube," *Applied Thermal Engineering*, vol. 30, no. 16, pp. 2505 – 2511, 2010.

[6] K. Wu, Z. Wang, X. Han, L. Tang, and M. G. Chen, "Working gases characteristics' influence on energy separation of vortex tube," in *10th IIR Gustav Lorentzen Conference on Natural Refrigerants*, no. GL-223. Delft, The Netherlands: Delft University of Technology, June 2012, pp. 912–919.

[7] R. Collins and R. Lovelace, "Experimental study of two-phase propane expanded through the Ranque-Hilsch tube," *Journal of Heat Transfer*, vol. 101, no. 2, pp. 300 – 305, 1979.

[8] Y. Liu and G. Jin, "Vortex tube expansion two-stage transcritical CO_2 refrigeration cycle," in *1st International Conference on Energy and Environmental Protection*, vol. 516-517, 2012, pp. 1219 – 23.

[9] T. Maurer, T. Zinn, and H. Sakashita, "Expansion device for working medium using vortex tube," 1999, DE Patent App. DE1,997,148,083.

[10] D. Li, J. Baek, E. Groll, and P. Lawless, "Thermodynamic analysis of vortex tube and work output expansion devices for the transcritical carbon dioxide cycle," in *4th IIR-Gustav Lorentzen Conference on Natural Working Fluids at Purdue, Purdue University, USA*, 2000, pp. 433–440.

[11] S. Elbel, "Experimental and analytical investigation of a two-phase ejector used for expansion work recovery in a transcritical R744 air-conditioning system," Ph.D. dissertation, University of Illinois at Urbana Champaign, 2007.

[12] S. Eiamsa-ard and P. Promvonge, "Review of Ranque-Hilsch effects in vortex tubes," *Renewable and Sustainable Energy Reviews*, vol. 12, no. 7, pp. 1822 – 1842, 2008.

[13] R. Tillner-Roth and H. D. Baehr, "An international standard formulation for the thermodynamic properties of 1,1,1,2-tetrafluoroethane (HFC-134a) for temperatures from 170 k to 455 k and pressures up to 70 MPa," *Journal of Physical and Chemical Reference Data*, vol. 23, no. 5, pp. 657–729, 1994.